This is to certify that the

thesis entitled

Experimental Investigation of the Flow Field in a Motored Rotary Engine Assembly

presented by

Emil N. Chouinard

has been accepted towards fulfillment of the requirements for

M.S. degree in Mech. Eng.

Harold Schock
Major professor

Date 7/05/90

EXPERIMENTAL INVESTIGATION OF THE FLOW FIELD IN A MOTORED ROTARY ENGINE ASSEMBLY

By

Emil N. Chouinard

A THESIS

Submitted to
Michigan State University
in partial fulfillment of the requirements
for the degree of

MASTER OF SCIENCE

Department of Mechanical Engineering

1990

ABSTRACT

EXPERIMENTAL INVESTIGATION OF THE FLOW FIELD IN A MOTORED ROTARY ENGINE ASSEMBLY

By

Emil N. Chouinard

Due to the complex nature of in-cylinder flows and the increasing use of complex computer simulations to predict engine performance, it has become necessary to understand thoroughly the characteristics of the fluid flow in the rotary engine combustion chamber. With this goal in mind, laser Doppler velocimetry and high speed flow visualization were used to study the flow patterns in a motored rotary engine assembly modified to allow optical access.

In the first part of the investigation, high speed film was taken in the engine at 675 rpm, in order to understand better the qualitative nature of the flow field and to locate regions of interest where LDV measurements could be made. Velocity measurements were then made to quantify the flow features of interest. Both the LDV and the flow visualization results revealed that the intake flow pattern was dominated by a large scale recirculation moving in the opposite direction of the rotor, which was caused by the interaction of the blowby jet, initiated by the apex seal separation, and the flow inducted through the intake port. The flow in compression was found to be predominantly pushed ahead of the rotor, but flow reversals were noted.

Next, in an attempt to study the in-cylinder flow at higher speeds, a high speed film was taken in the engine at a speed of 2000 rpm. This film revealed that the flow patterns varied very little at the higher speed.

ACKNOWLEDGMENTS

I would like to take this opportunity to thank several people whose help was invaluable in completing this work. First, my advisor Dr. H. Schock for his technical assistants and also for making working at the MSU Engine Lab enjoyable; to Dr. F. Hamady for his countless hours of instruction on the LDV system; to my committee members, Dr. M. Koochesfahani and Dr. C. Somerton for their helpful comments; and to all my friends in the engine lab group for contributing to lunch time comedy hour.

I also would like to express my gratitude to NASA Lewis Research Center for their financial support.

TABLE OF CONTENTS

LIST OF TABLES

LIST OF FIGURES

Page

LIST OF SYMBOLS

λ - Wavelength of laser light

d - Laser beam spacing

f - Focal length of transmitting lens

l_m - Length of measurement volume

d_m - Width of measurement volume

d_f - Fringe spacing

κ - Half angle between beams

V - Velocity of particle as determined by Doppler shifting

F - Doppler frequency

U_{mean} -Ensemble average mean velocity

U_{RMS} -Root Mean Squared (RMS) velocity

α - Crank angle

Σ - Summation from i =1 to N

N - Number of cycles

τ - Relaxation time of the particle

T - Lagrangian macro-time scale of the turbulence

ρ_p - Particle density

d_p - Particle diameter

η - Average gas viscosity

ε - Momentum eddy diffusivity

v' - Turbulence intensity

μ - Turbulence viscosity

K.E. - Turbulence kinetic energy

CHAPTER 1

INTRODUCTION

1.1 Problem Statement

The rotary combustion engine (RCE), since the first working design was introduced, has had a loyal group of supporters who are keenly aware of its advantages over traditional power plants. In the earlier days of its development, many of these supporters expected the rotary engine to revolutionize the automotive industry and virtually replace the reciprocating piston engine. However, this never happened due to some inherent difficulties related to the engine design. However, the rotary engine's design advantages have given it a place in special applications as will now be discussed.

First, in terms of fuel consumption and specific weight, the rotary combustion engine seems to fit between the small gas turbine and the reciprocating piston engine. The rotary engine's fuel consumption is slightly higher than that of the piston engine; however, it is substantially lower than that of the simple small gas turbine. In terms of power-to-weight ratio and volume, the rotary engine has a higher power density than that of the piston engine and a poorer power density than that of the turbine engine. The rotary engine has two other important advantages: unlike the piston engine, it can maintain its power density on a variety of fuels including readily available jet fuel and, unlike the turbine, it can maintain its performance under high altitude conditions.

The application for which the rotary engine is clearly a superior choice over piston and turbine engines is low power aircraft propulsion. Another important application which has received a significant amount of attention is the use of the stratified charge rotary engine (SCRE) as an auxiliary power unit for large commercial and military aircraft. Significant interest also exists in using natural gas-fueled rotary combustion engines as replacements for large electric motors. The compact size of the rotary engine and its potential for long life make this possible from an economics standpoint.

Recognizing the potential nonautomotive applications for the rotary engine, Mazda has recently made available a two-rotor homogeneously charged rotary engine as a stand-alone power plant. This is the engine that they presently mass produce for their sports car.

Deere & Co. has demonstrated that the stratified charge rotary engine can develop the predicted power density of 4BHP/ci displacement. Although the rotary engine has a number of demonstrated advantages for the applications described above, before an engine can be put into even small scale mass production, it must have clearly demonstrated that it is superior to commercially available power plants. Hamady et al [1] estimate that a 25% improvement in the thermal efficiency of the stratified charge rotary engine is necessary before commercialization of the engine will be feasible. An improved combustion system design would be a key contribution to this increased efficiency.

With the goal of improving the combustion system of the rotary engine, the objective of current research is to develop an understanding of air flow, fuel-air mixing, and combustion phenomena in the stratified charge rotary engine. This information will then be used to suggest design changes which will enhance the fuel economy and power density of the rotary engine.

This investigation will give results that reveal some of the important flow structures in the compression and intake stroke of the rotary engine. The velocity measurements were made with a laser Doppler velocimeter (LDV). However, flow visualization using a high speed camera at 5000 frames per second (fps) was first conducted to obtain a good understanding of the flow structure was obtained. The films were used to identify flow structures of interest that could be quantified with LDV measurements. They also allowed the results of the velocity measurements to be visually confirmed.

1.2 Literature Survey

At the early stage in the design process of the rotary combustion engine, little consideration had been given to systematic study of the influence of the controlling parameters on the fluid flow, air-fuel mixing and combustion process. Most of the works were limited to test performance, level of durability and environmental emission standards [2-4].

Evaluations of the effect of apex and side seal leakages on the Mazda R-100 rotary engine performance was presented in work by Eberle and Klomp [5] . The authors compared experimental and computational results and predicted that significant gains in engine performance could be achieved, depending on the leakage reduction and the operating conditions. However, they used an effective leakage area that was constant with rotor position, which is not supported by experimental observations. Therefore, their predicted performance gains may be high.

Noting the importance of the seal leakage, Knoll et al [6] studied the dynamic behavior of the rotary engine seals. This study indicated that accurate pressure measurements are needed at the seals to predict the dynamic behavior of the seals. However, when an average cell pressure was used reasonable results were obtained. Their study predicted seal separation as was known in the real engine.

Meng et al [7] investigated the possibility of using turbocharging on a rotary engine, to improve brake specific fuel consumption (BSFC) and the specific weight. The results showed a power increase of 36 percent with turbocharging at 5900 rpm with 7 psi of boost. However, the engine showed a relatively low thermal efficiency of 29 percent, compared to 40 percent for available diesel engines. The low efficiency was attributed to slow combustion, and the authors predicted that an increase in efficiency will require controlled combustion, improved thermal barriers and advances in sealing technique.

These earlier studies led to the conclusion that detailed investigation of the flow field in the rotary engine was necessary to predicate the design changes needed to improve the rotary engine's thermal efficiency, fuel consumption, and emissions performance. To this end, several attempts at developing a computer code that could model the complex flow in the engine were conducted.

A one-dimensional model for the combustion process was developed by Bracco and Sirignano [8] based on the use of turbulent diffusivity. Results indicated that theoretical design changes could be tested for their affects on engine performance. However, owing to the complex interactions of the various controlling factors, more analytical and experimental studies were necessary for reliable predictions to be made.

Shih, Yang and Schock [9] made the first attempt at using a two-dimensional model to predict fluid flow in the rotary engine. The results were promising, in that they seem to suggest that the operating parameters could be changed to study their effect on engine performance. However, the authors noted the limitations of a two-dimensional model. In particular, its inability to model cross flow jets, as would be present in fuel injection, and Taylor vortices, which were known to occur in real engines.

Again using a two-dimensional model, Shih, Schock and Ramos [10] investigated fuel-air mixing and combustion in a direct-injected stratified-charge (DISC) rotary engine. The results indicated that when a gaseous fuel was injected the mixing and fuel penetration increased with injection velocity, however, in general, the fuel penetration was poor. The poor penetration was attributed to the planar geometry used and the gaseous fuel injection jet, which does not penetrate as well as a liquid jet due to the difference in density.

Recognizing the need for a more sophisticated code, Steinthorsson et al [11] developed a three-dimensional code to study the fluid flow in the rotary engine. This code again predicted poor gaseous fuel penetration during the injection event, but more importantly it moved one step closer to modeling the complex flow in the rotary engine.

In conjunction with the computational studies, experimental investigations of the flow field have been conducted in order to verify assumptions that have been made in numerical simulations and to provide more details of the flow characteristics.

Holographic interferometry was used to study small and large scales of the flow structures in the intake by Hicks et al [12]. Helium was injected with the entrained air so that fringe patterns could be recorded which allowed density variation measurements of the flow field.

Dimpelfeld and Witze [13] is the only reported study that has done LDV measurements in the rotary engine. In their investigation, limited measurements were taken in the intake manifold, intake and exhaust strokes of a 5.81 liter motored rotary engine. The engine was run with a sacrificial oil that caused window fouling; therefore, to avoid complexity the LDV system did not use frequency shifting. Hence, the system could not measure flow reversals which the present study shows can have a significant influence on the flow patterns during the intake and possibly the compression strokes. Dimpelfeld and Witze presented measurements in the intake stroke that showed a sharp peak in the tangential velocity (tangent to the central housing) near the intake port. Measurements made in the present study in a similar location suggest that this sharp peak in velocity during intake may have been caused by the blowby jet flow that was actually moving opposite to the rotor motion, but could not be measured as such with the system used in the study. Measurements made in the compression stroke indicated that the flow was predominantly pushed ahead of the rotor and turbulence intensities were much more uniform than those seen in the intake stroke. These results are supported by the present study.

Hamady, Stuecken, and Schock [14] presented detailed flow visualization results for the same modified rotary engine used to make the LDV measurements presented in this investigation. These high speed films were used to investigate in-cylinder flow patterns in the intake and compression stroke under naturally aspirated and supercharged conditions, at speeds of 675 and 1170 rpm. The flow visualization results for all the conditions tested indicated that there was a substantial amount of blowby past the apex seal. The central housing used in the study had a window modification in the central housing, which could have been the cause of the leakage past the apex seals. Therefore, LDV measurements made in this study were made without the window modification.

The objective of this work is to develop an understanding of the controlling factors that affect the SCRE combustion process so that an efficient, power dense rotary engine can be designed. The influence of the induction-exhaust systems and the rotor geometry are believed to have a significant effect on the combustion chamber flow characteristics In this study emphasis was placed on LDV measurements in the combustion chamber of a motored rotary engine assembly. This will provide a basic understanding of the flow processes and complement flow visualization. This information will serve as a data base for verification of numerical simulations.

The remainder of this work will be arranged as follows: First experimental facilities and procedures will be discussed; then the results will be reviewed, followed by summary and conclusions. Finally recommendations for future work will be presented.

CHAPTER 2

EXPERIMENTAL FACILITIES AND PROCEDURES

2.1 Experimental Facilities

2.1.1 Laser Doppler Velocimeter

The laser Doppler velocimeter (LDV) consists of a 4 watt argon-ion laser manufactured by Coherent, optical and signal processing equipment designed and built by TSI, Inc. and an IBM PS/2 80 computer for data acquisition. The system is currently operating in single-line mode, allowing the measurement of one velocity component at a time. A schematic of the LDV is shown in Figure 1, and a photograph of the experimental setup is shown in Figure 2.

The laser, transmitting optics and the receiving optics are mounted on a rigid traverse table, Model 9900-1, specifically designed for traversing a LDV optical system, as shown in Figure 3. This method of traversing the system allows flexibility in relocating the measurement volume within the chamber, as the distance from the focusing lens and the measurement volume remains fixed. Translation in three directions (x,y,z) is achieved by a hand held electronic controller. The laser is manufactured by Coherent, Model 90. It is operated in the green-line, wavelength 514.5 nm. The specifications of the laser system is given in Table 1.

Table 1 LDV Specifications

Laser wavelength (λ)	514.5 nm
Laser Power	0.4-1.0 W
Beam Spacing	22 mm
Transmitting Lens Focal Length (f)	250 mm
Collecting Lens Focal Length	250 mm
Length of Measurement Volume (l_m)	3.89 mm
Width of Measurement Volume (d_m)	164 um
Fringe Spacing (d_f)	1.12 um
Half Angle Between Beams (κ)	2.41 deg
Number of Fringes	28

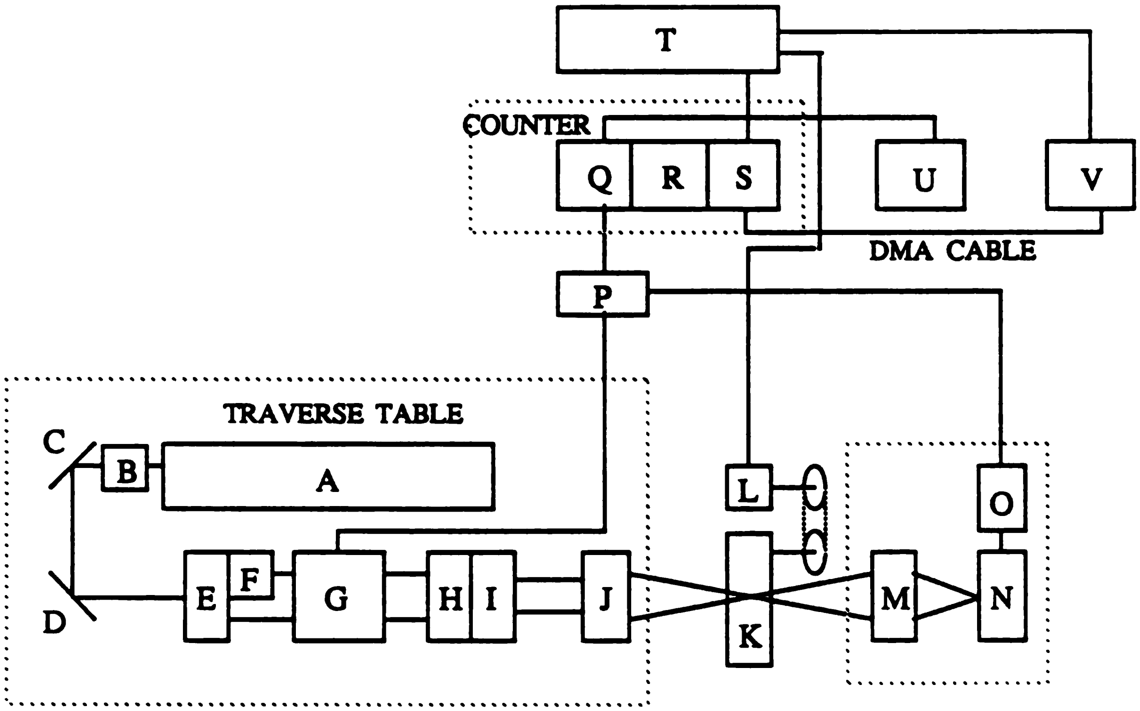

A) ARGON-ION LASER
B) COLLIMATOR
C) STEERING MIRROR
D) STEERING MIRROR
E) BEAM SPLITTER
F) POLARIZER
G) BRAGG CELL
H) BEAM STOP
I) BEAM SPACER
J) TRANSMITTING LENS
K) ROTARY ENGINE ASSEMBLY
L) BEI SHAFT ANGLE ENCODER
M) COLLECTING LENS
N) RECEIVING MODULE
O) PHOTOMULTIPLIER
P) FREQUENCY SHIFTER
Q) INPUT CONDITIONER
R) TIMER
S) MASTER INTERFACE
T) ROTATING MACHINERY RESOLVER
U) OSCILLOSCOPE
V) IBM PS/2 80 COMPUTER

Figure 1 Schematic of laser Doppler velocimeter

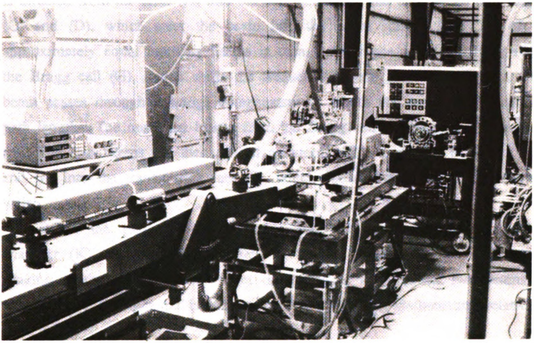

Figure 2 Laser Doppler velocimeter and rotary engine assembly

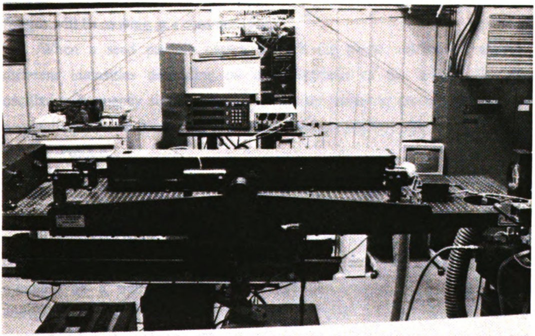

Figure 3 Traverse table

Referring to Figure 1, the system operates as follows. The coherent light source is directed from the laser (A) into the collimator (B), and then to the directing mirrors (C) and (D), which steer the beam into the beam splitter (E). One of the two approximately equal intensity beams is then fed into the polarizer (F) and then into the Bragg cell (G), which shifts the frequency of one beam by 40 Mhz. The other beam passes through a wedge compensator to assure the beams travel equal optical path lengths. The unshifted beams from the Bragg cell are blocked by the beam stop (H). The two beams are then spaced a determined distance by the beam spacer (I) and fed into the transmitting lens (J), which causes the beams to intersect at their waist.

When the two coherent beams intersect in the rotary engine combustion chamber (K), an interference pattern of equally spaced fringes is produced. The spacing of the fringes is dependent on the angle between the two beams and the wavelength of the light, and is represented by the following mathematical relation,

$$d_f = \lambda/2\sin\kappa$$

where d_f is the fringe spacing, λ is the wavelength of light, and κ is the half angle between beams. A diagram illustrating these parameters is shown in Figure 4. These fringes would normally be stationary. However, when the Bragg cell is used the fringes will be moving at a constant speed.

When a seed particle passes through the probe volume, it scatters light at different intensities depending on the brightness of the fringe. This produces a oscillating frequency signal that can be directly related to the velocity, in the direction perpendicular to the fringe pattern, by the following relationship,

$$V = d_f \times F$$

where V is the velocity of particle, and F is the doppler frequency. The movement of the fringes in one direction allows the directionality of the velocity to be determined.

The scattered light from the seed particles is collected by the photomultiplier (O), with the aid of the receiving optics (M) and the receiving module (N), which are mounted on a rigid arm extending from the traverse table. The photomultiplier converts the light intensity into an electric signal, with a frequency that is linearly proportional to the velocity. This frequency signal is then sent to the frequency shifter (P). The frequency shifter allows the adjustment of the zero velocity reference frequency, which allows the directional nature of the flow to be determined.

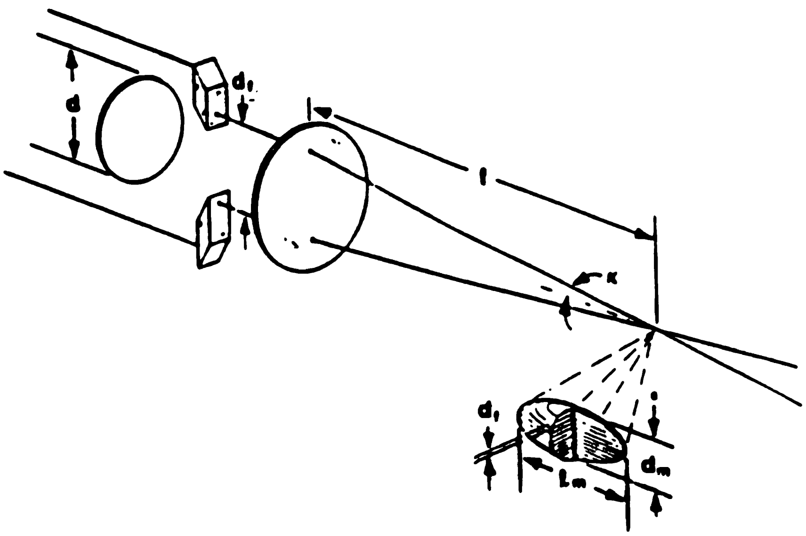

Figure 4 Diagram illustrating the systems optical parameters

This signal is then sent to a counter type processor, TSI Model 1990, which is comprised of three components; the input conditioner (Q), timer (R), and the master interface (S). The counter makes measurements on a frequency burst by measuring the time for N cycles of the burst at a maximum sample rate of 5 KHz. The input conditioner makes an envelope of the time to be measured, and the timer measures this envelope by utilizing a high speed clock.

The first function of the input conditioner is to amplify and filter the input signal. Signals from the LDV generally have a DC component or "pedestal". However, for the trigger to operate properly, the frequency burst must be symmetrical about a fixed level. The low limit filters are necessary in most cases to remove this DC component. The high limit filter is used to filter out high frequency noise from the input signal. Output accuracy depends on the signal-to-noise ratio of the signal entering the trigger, so extraneous noise should be filtered as well as possible. The filtered Doppler signal can be viewed on the oscilloscope (U) to examine its quality.

The function of the timer is to measure the length of the envelope provided by the input conditioner. The leading edge of the envelope gates a high speed clock (250 MHz) into the counter. The trailing edge of the envelope stops the counter. The number in the counter is then the measure of the length of the envelope, with a resolution of 1 ns.

When the signal processor records velocity data from a particle in a fluid, a signal is sent to the Rotating Machinery Resolver (RMR) (T) that causes it to latch "hold" the angular position of the shaft angle encoder at the same instant. This position information is then passed with the velocity data to the IBM PS/2 80 (V) computer via the master interface unit.

The master interface controls the flow of data in the system. All data transferred to the computer by the DMA controller passes through, and is controlled by, the master interface. The master interface transmits control signals and data to the DMA controller in the computer and, in turn, receives control signals from the DMA controller.

The shaft angle encoder is connected to the crank shaft of the rotary engine, via a gear and belt mechanism, which is shown in Figure 5. The encoder puts out 1024 evenly spaced pulses per revolution. This resolution can be multiplied by a factor of 2 or 4 in the software.

In many situations the study of the flow in a device is limited to certain times or positions in the rotation, for example, when the rotor is not physically blocking the measurement volume. Since storing LDV data from the entire cycle and then rejecting the data from unwanted locations would result in a significant waste of computer memory space and computing time, the resolver can be used to enable the signal processor for strictly designated "windows" or "gates" in the rotational cycle. These windows can be set at any angular position throughout the revolution, and the width of each window can be designated.

This system allows the measurement of velocity-encoder position data pairs, which can be sent to the PS/2 80 IBM computer, where the raw data can be manipulated using the TSI Rotating Machinery Program (RMP) software design to handle this type of test setup. Figure 6 shows the counter processor, the RMR, the oscilloscope and the computer used in the experiments. The RMP program allows the calculation of the ensemble averaged mean and RMS velocity as a function of crank angle degree (cad).

2.1.2 Rotary Engine Assembly

The rotary engine operates differently than does the piston engine in a basic way. Unlike the reciprocating piston engine, the rotary engine transmits power to the crank shaft directly by rotating and translating on the crank shaft itself. The power is delivered to the crank shaft by generating torque via an eccentricity of the rotor as the rotor gear walks on the stationary gear on the crank shaft, as shown in Figure 7. The intake and exhaust are fixed openings on the central housing and the intake, compression, and exhaust cycles occur at the same time in three distinct chambers defined by the three-lobed rotor and the tricoidal shaped central housing. This configuration gives three power strokes for every one revolution of the rotor, which is one of the reasons for the engine's high power density.

In order for the rotary engine to perform properly, the three chambers must be sealed off from one another. This is accomplished by using a sealing grid as shown in Figure 8. The six side seals, three on each side of the rotor, ride in spring-loaded grooves and seal the area between the side housing and the side of the rotor. The apex seals also ride in spring-loaded grooves across the top of the apices of the three lobes. These seals seal the area between the rotor face and the central housing at the lobe apices where the two rotor flanks meet. The button seals are round cylindrical

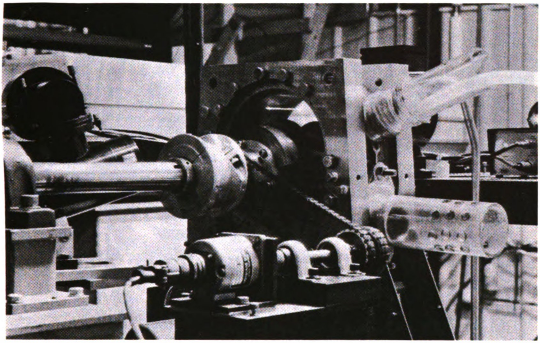

Figure 5 Shaft angle encoder driven by the rotary engine

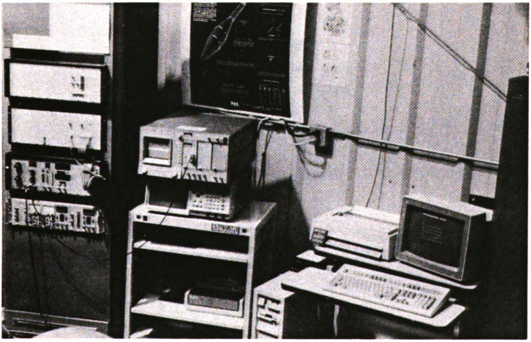

Figure 6 Data acquisition system for LDV measurements

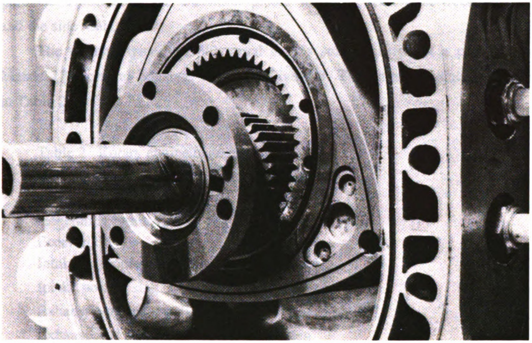

Figure 7 Stationary and rotor gear used to transmit power to crank shaft

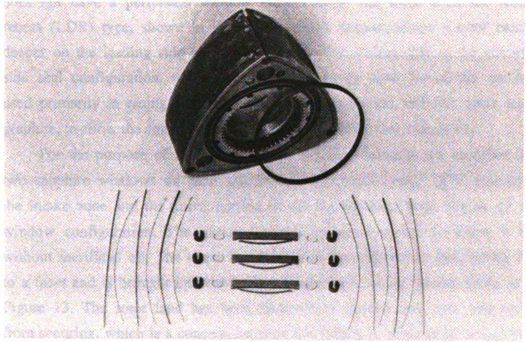

Figure 8 Sealing grid used in the rotary engine assembly

pieces with a slot to accommodate the apex seals, and they also ride in spring-loaded grooves. These seals are transition pieces to allow sealing between the apex seals and the side seals.

The rotary engine assembly used in this study consists of a peripherally ported Mazda 12A central housing, shown in Figure 9. The engine characteristics are given in Table 2.

Table 2 Rotary engine characteristics

Major axis (y)	120 mm
Minor axis (x)	90 mm
Generating radius (R)	105 mm
Eccentricity (e)	154 mm
Intake port opening (IPO)	267 deg
Intake port closing (IPC)	350 deg
Exhaust port opening (EPO)	12 deg
Exhaust port closing (EPC)	66 deg

The engine is motored by a 7.5 kW (10.0 hp) constant torque electric motor. The central housing used for the velocity measurements is a production type; therefore, it does not have a peripheral window modification. The rotor is of the leading deep recess (LDR) type, shown in Figure 10, which accommodates a rotor recess that is deeper on the leading side of the rotor face. The sealing grid is the common single side seal configuration, while the apex seals being used are of the one-piece type used primarily in racing engines. The apex seals, button and side seals are made of graphite, to allow the engine to run without sacrificial oil (see Figure 11).

For the purpose of the present study, the side housings are modified to support two sapphire windows on each side to allow forward scatter LDV measurements in the intake zone and the upper portion of the compression zone. Figure 12 shows the window configuration. The motored engine is water cooled to allow it to be run without sacrificial oil. The water is delivered to the engine by tygon tubing hooked up to a facet and is brought into the engine by the steel tubing modification, as shown in Figure 13. The rotor land has been removed to prevent the rotor and side housing from scouring, which is a concern since no lubrication is being used during the motored operation. The land is a projection on the side face of the rotor that centers the rotor between the two side housings, and maintains proper clearances between the two

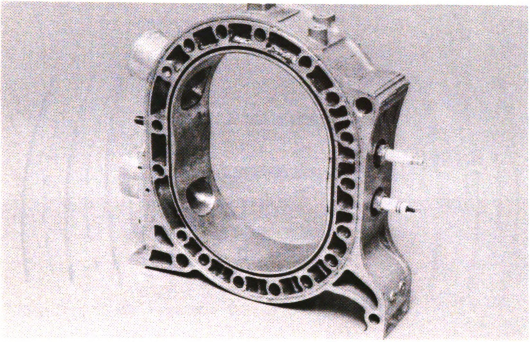

Figure 9 Mazda 12 A central housing used in the test engine

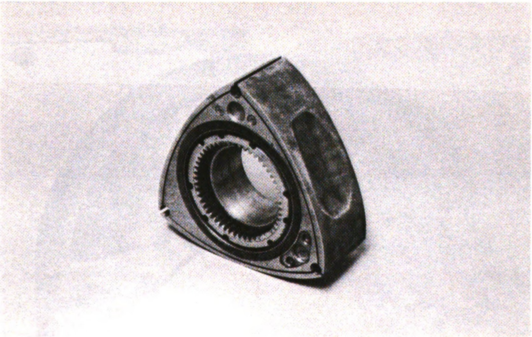

Figure 10 Leading Deep Recess rotor used in the test engine

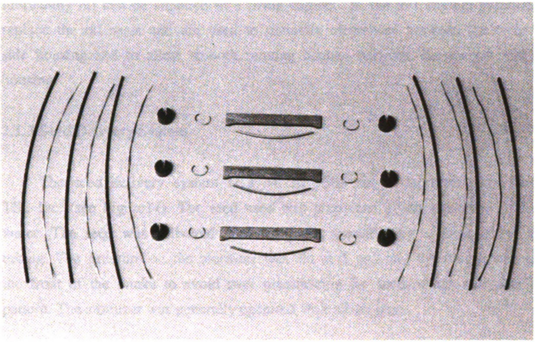

Figure 11 Graphite seals used to run the engine without lubrication

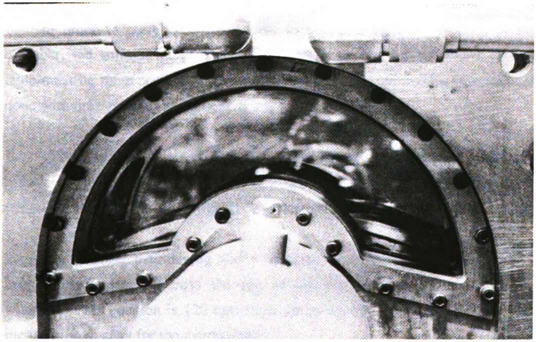

Figure 12 Window configuration used to gain optical access

surfaces. It is generally located on the inner side of the oil seal where sufficient lubricating oil can be supplied in a firing engine. In the test engine, graphite spacers replace the oil seals and are used to maintain clearances between the rotor and the side housing and to allow smooth running contact between the spacers and the side housing.

2.1.3 Seed Delivery System

The seed delivery system is a Model 9306 six-jet atomizer manufactured by TSI, Inc. (see Figure14). The seed used was propylene glycol dissolved in 5 parts of water. The seed was delivered into the intake manifold by a short length of tygon tubing. The pressure on the atomizer was set at 5 psi, and the tubing was placed at the front of the intake to avoid over pressurizing the seed, which can alter the flow pattern. The atomizer was generally operated with all six jets.

2.2 Experimental Procedures

2.2.1 Traverse Table Reference

In order to correlate measurement locations to distinct positions in the engine chamber, the traverse table must be referenced on the rotary engine assembly. The table must be referenced in the three directions of x,y, and z. This procedure should be done with the beams forming a horizontal plane.

1. The y reference is set by focusing the beam crossing on the major axis of the rotary engine, which is located by the center hex nut used to secure the sapphire windows. The readout of the y position is then set to zero on the position display box.

2. Then, while maintaining the y direction zero, the table is lowered until the beams just appear to cross the top of the central housing through the sapphire windows. This position is 120 mm from the minor axis and can be entered as such on the position display for the z direction.

3. The x direction reference is determined by focusing the beam crossing on the

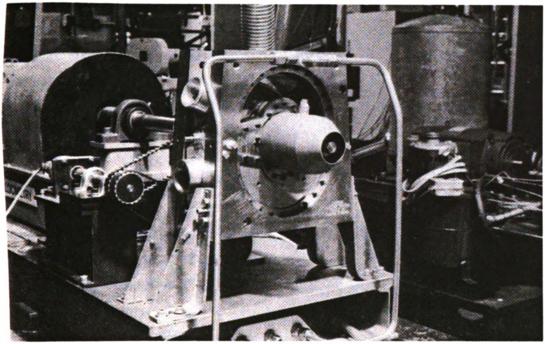

Figure 13 Tubing system used to deliver cooling water

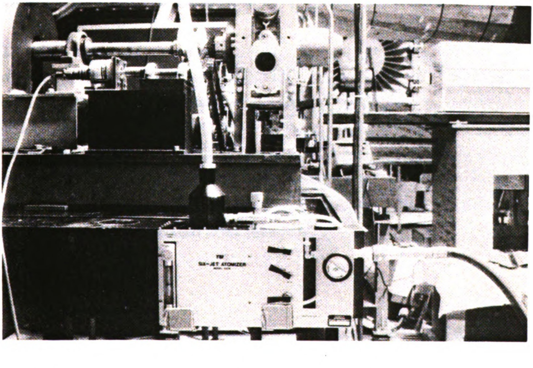

Figure 14 Six-jet atomizer used to deliver seeding to the rotary engine

inside of the surface of one of the sapphire windows. This can sometimes be difficult, with the exact focus being ambiguous, therefore, an alternative method can be used. This method involves filling the chamber with seeding particles with the output of the Doppler signal displayed (see the section on focusing the optics) on the oscilloscope. Then the control volume can be moved slowly into the chamber until a good Doppler signal can be seen. The inside surface of the window is 35.0 mm from the center line of the central housing, and is entered as such on the position display box.

2.2.2 Shaft Angle Encoder Reference

In order to obtain valid velocity versus crank angle position data, the encoder must be referenced to a known position of the crank shaft, or the rotor, which makes a third of a revolution for one revolution of the crank shaft.

1. First, the rotor must be placed in a known position, usually by placing the apex seal of one of the rotor lobes at the top of the mouth of the intake port, which is at the very beginning of compression. For all of the velocity measurements presented in this paper, the three chambers were considered identical, therefore, the choice of lobes is irrelevant, providing all the seals are operating the same.

2. The output of the encoder, which puts out a high reference signal every revolution, must then be synchronized with the rotor position chosen. This is done by displaying the output of the window monitor of the RMR on an oscilloscope that can clearly detect a 5 volt signal. Then the window size must be adjusted in the RMP software to a sufficiently small value as to get an accurate reference. For the present study it was set at 4 encoder positions, or 0.68 degrees. Then, by rotating the flexible coupling on the shaft angle encoder and stopping when the high reference pulse can be seen, the encoder is referenced to the rotor position.

2.2.3 Focusing the optics

Before the velocity measurement can be made, an acceptable Doppler signal must be obtained by properly focusing the receiving optics for the photomultiplier. This is done in the following way.

1. The receiving optics are adjusted with the slot on the base plate, shown in Figure 15, until the front of the receiving optics is approximately 25 cm (the focal distance of the receiving optics) from the measurement volume. The measurement volume can be placed in the desired location inside the chamber of the rotary engine.

2. The chamber is then filled with seeding particles and sealed. The crossing can be viewed through the eye piece, which is placed on the mount for the photomultiplier (see Figure15). The beam crossing is focused by first making rough adjustments with the base plate, which allows rotation around the securing bolt and translation along the slot. The crossing should be fairly well focused and centered in the eye piece when the fine adjustments are made with the sliding adjustment on the focusing lens. Once the crossing is focused it can be centered exactly by using the fine adjustment wing nuts on the base of the mounting tube. Ambiguity in focusing is encountered when the crossing is viewed in the same plane that the two intersecting beams form. The crossing, when seen from this angle, appears as an hour glass, which is very hard to focus accurately. This problem is overcome by lowering the mounting plate with respect to the table and angling the receiving optics appropriately, with the modified base. From this angle the crossing is clearly seen as the intersection of two distinct beams.

3. The final check on the focusing is done while viewing the data rate on the counter and the Doppler signal on the oscilloscope. The fine adjustments are made until the data rate and the signal quality are optimized.

2.2.4 Signal Conditioning

The Doppler signal, after leaving the photomultiplier, can be manipulated at several stations before it is converted to velocity-crank angle data pairs and sent to the computer for statistical manipulation. The signal is conditioned in the following ways.

1. The signal can be amplified at two locations in the system. The first amplification is performed at the power supply for the photomultiplier. The signal can also be amplified at the gain control on the input conditioner of the counter. The gains

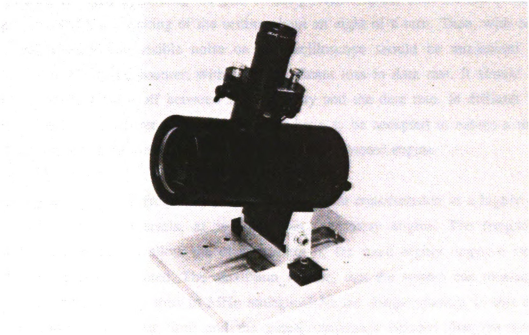

Figure 15 Optics used to collect and focus the measurement volume

are set to optimize the data rate while minimizing the noise in the Doppler signal. This is best done by turning the gain on the photomultiplier until the red overload light goes on and then backing of the setting about an eight of a turn. Then, with one of the beams blocked the visible noise on the oscilloscope should be minimized with the gain control on the counter, without a significant loss in data rate. It should be noted that there is a trade off between signal quality and the data rate. In difficult locations in the engine, a poorer signal quality may have to be accepted to assure a reasonable data rate, which minimizes the running time of the motored engine.

2. An appropriate frequency shift is an important consideration in a highly turbulent flow, with flow reversals, as is present in the rotary engine. The frequency shift should be chosen to allow the measurement of the most highly negative velocity in the flow that is expected. The maximum velocity that the system can measure in m/s will be the frequency shift in MHz multiplied by the fringe spacing, in this case 6.12 um. This is the lower limit and the actual maximum velocity that the system can measure will be slightly less. The prediction of the maximum negative velocity expected in the flow in the rotary engine is not obvious, therefore, it is advisable to make test runs at different shifts. The method of determining the suitability of the shift value will be discussed in the section on data acquisition.

3. After the shift has been chosen at a particular location in the engine chamber, the signal can be filtered by adjusting the low and high filters on the input conditioner of the counter. Of course, the filters must be adjusted so as to allow the shifted frequency to pass through the system, while eliminating high and low frequency noise. The high frequency filter should be set to allow the maximum expected positive velocity. Again the maximum velocity the system can measure will be the difference between the high frequency filter setting and the frequency shift setting multiplied by the fringe spacing, The low frequency filter should be set to allow the maximum negative velocity determined by the frequency shift to pass through the system, as discussed above.

4. Another parameter that can be adjusted on the input conditioner is the minimum number of burst counted in a cycle. This determines the number of cycles that will be counted in the burst to determine the velocity of the particle. The more cycles that are

counted, the more stringent the acceptance criteria, which results in a decline in the data rate. For the present study, this value was maintained at 8 burst per cycle for all of the measurements.

2.2.5 Data Acquisition and Reduction

After the measurement location is determined and a good signal is obtained, parameters in the TSI RMP software must be set. The software has four basic modules which are: (1) Data Acquisition (2) Statistical Analysis (3) Velocity Histogram (4) Data Display. Only the parameters that are directly related to data acquisition and reduction will be discussed. For a more detailed description of the settings see reference [15].

1. In the RMP software, the first parameters to be set are the acquisition parameters. In this study, the amount of data collected was decided by the number of words, as opposed to taking data a fixed length of time. The number of words collected can range from 1 to 5 million, but due to the fact that the velocity- crank angle data pair is three words in length the actual number of measurements is a third of the number specified in the software.

2. The counter parameters must then be set to match the external settings on the hardware. The n-cycle exponent is set to match the burst per cycle setting on the input conditioner of the counter. These values will be expressed as the value of two raised to an exponent. The frequency shift software setting is set to match the shift chosen on the frequency shifter. The fringe spacing is set at the value determined by the calculation already discussed. In this study this value remained at 6.12 um.

3. The rotary encoder parameters to be selected are as follows. The software resolution, which determines the size of the window that the ensemble averaged velocity will be averaged over during a cycle. The number of encoder points per revolution is 2048. This value is determined by multiplying the number of pulses that the encoder emits per revolution, which is 1024, by the multiplication factor of two, which is set by highlighting the shaftencoderX2 selection. This gives 2048 encoder points per revolution, which represents the maximum resolution that the software can

achieve. 2048 encoder positions is equivalent to 360 cad. The number of encoder points per blade is chosen to equal the encoder points per revolution. For an explanation of different uses of this parameter see reference [15]. The number of encoder points per window controls the size of the window over which the data will be taken, and it can be set between the software resolution and the encoder points per blade.

4. The statistical analysis module is used to convert the raw data files into usable velocity versus crank angle data. The velocity statistics of interest are the ensemble average velocity and the root mean squared (RMS) velocity, which can be represented mathematically as follows,

$$U_{mean} = 1/N \, \Sigma \, V_i (\alpha)$$

$$U_{RMS} = (1/N \, \Sigma \, (V_i (\alpha) - U_{mean})^2)^{1/2}$$

where U_{mean} is the ensemble averaged mean velocity, U_{RMS} is the root mean squared velocity, $V_i (\alpha)$ is the instantaneous velocity of the i $_{th}$ cycle, and α is the crank angle.

The ensemble averaged velocity is phase averaged over the number of cycles of the engine and is also averaged over the software resolution. The RMS velocity is a measure of the intensities of the fluctuations, from cycle-to-cycle, of the averaged quantity.

5. The velocity histogram module allows the user to calculate the density distribution of the velocity data at a specific cad. This distribution should be approximately Guassian in shape, with a lack of symmetry indicating possible mistakes in the choice of frequency shift or the filter settings.

6. The data display module allows the velocity-crank angle and the density function plots to be displayed, which can be an immediate check on the validity of the measurements.

2.2.6 Measurement Procedure and Validation

In order to assure that the measurements being collected were correct or at least reasonable, several checks on the data were performed.

1. The measurements were taken at two frequency shifts, usually 5 and 10 MHz, at the same location and operating conditions, in order to verify that the shifting did not have a significant effect on the measurements. This procedure was continued until a pattern developed indicating expected flow behavior. Usually, the first three or four locations were duplicated.

2. The density distribution at difficult locations (in highly turbulent regions or in windows with large flow reversals) has to be approximately Guassian in shape, without any obvious indication of frequency biasing or filter cut-off.

3. To assure that the data are continuous and repeatable, each encoder position (approximately 0.18 cad) had to contain at least 100 data points. Near the rotor edge, as the rotor approached the control volume, this value was sometimes lower, but no data was accepted that contains less than 60 data points. The window resolution was set at 2.85 cad, which resulted in smooth plots while not losing the character of the plot.

4. Finally, and perhaps most significantly, all the velocity measurements were checked for directional validity with the high speed film. All of the measurements presented in the present study were confirmed to be qualitatively correct by visual observation.

2.2.7 Test of Seals

In order to determine if the test engine was sealing properly, two types of pressure tests were performed. First, a stationary test was completed with the setup shown in Figure 16. First the rotor is placed at Top Dead Center (TDC). Then the pressurized feed line is hooked up to the stationary pressure test gauge, specifically designed for testing leakage in the rotary engine. When the stationary pressure test was performed there was a pressure drop of 186.3 kPa (27.0 psi), from 448.4 kPa (65.0 psi) on the feed line to 262.2 kPa (38.0 psi) on the compression chamber gauge. The pressure drop of 186.3 kPa (27.0 psi) indicated a somewhat ineffective sealing mechanism considering that the pressure drop on a Mazda production engine was only 48.3 kPa (7.0 psi). Therefore, an attempt was made to isolate the leakage. When the side seals were sealed using a silicon product, the pressure drop was reduced to 27.6 kPa (4.0 psi), which led to the conclusion that the majority of the leakage was due to the side and button seals and not the apex seals. Therefore, an attempt was made to quantify the velocity of the jet leaking past the apex seals, which is almost certainly a concern for production rotary engines. In fact, an acceptance test for the apex seals, taken from a Mazda repair manual [16], allows a clearance of 0.06 mm (0.0024 in) between the apex seals and the central housing, in a worst case scenario. This indicates that leakage is accepted in the rotary engine and, therefore, needs to be quantified experimentally.

The motored pressure test consisted of measuring the chamber pressure in compression as the engine was being motored. The pressure traces taken at 250 rpm gave a peak pressure of 586.4 kPa (85.0 psi), which was comparable to the results obtained for Mazda production rotary engines, as indicated in the Mazda repair manual referenced above. The pressure results further support the conclusion that the test engine sealing mechanism is comparable to the production engine. Similar tests were performed using two-piece metal apex seals, and the results confirmed that the test apex seals were performing as well as the production seal configuration.

After the velocity measurements were taken at 675 rpm with the graphite seals, experiments were conducted in an attempt to find a better sealing material. The first material tested was Teflon, which proved to be better at sealing in the stationary pressure test. However, when the engine was motored it tended to smear and deform. Next, ultra high molecular weight polyethylene was tried with similar results as stated above. The final material tried was nylatron GS, which contains molybdenum disulfide as an additive. This material did not seal as well as the graphite, and when the engine was motored at higher speeds thermal expansion caused the electric drive motor to stall due to the increase in the frictional force.

2.2.8 Seeding Experiments

An important consideration in LDV measurements is the selection of a seeding material. The particles used for seeding must be small enough to follow the fluid flow and not cross more than one fringe at once. Also, they must not cause window fouling, which results in a loss of optical access. The seed must also provide good data rates at reasonable concentration levels. Several different seeding particles were tested and these are listed below.

1. Dioctyl Phtalate (DOP)
2. Mineral Oil
3. Titanium Dioxide
4. Propylene Glycol

The DOP, due to its higher viscosity, caused considerable "fogging" of the windows, therefore, it was not suitable for use in this application. The mineral oil also caused a film to form on the windows and, therefore was not acceptable. The mineral oil also had the disadvantage of separating out of a water solution, which causes problems when using a diluted solution. The titanium dioxide also was unsuitable because of window fouling, which was largely attributed to the fact that the solid particles adhered to the wet surface of the window. Propylene glycol was found to be a very good seeding material, in that it caused little window fouling. It also mixed well with water and provided a good data rate. It also served a secondary purpose of providing lubrication for the motored engine, although this effect was not relied upon.

As stated earlier, the seed particles used for LDV measurements must not overlap on the fringes and must follow the smaller scales of the flow. The particle size distribution for propylene glycol is shown in Figure 17. The geometric diameter of propylene glycol is estimated to be 0.6 μm [17], which easily satisfies the first condition. In an analysis similar to that given by Regan, Chun, and Schock [18], a practical limit of $\tau / T \leq 0.02$ will ensure that the particles are essentially following the flow, where τ is the relaxation time of the particle and T is the Lagrangian macro-time scale of the turbulence. The particle relaxation time is given by,

$$\tau = \rho_p d_p^2 / 18 \eta$$

where ρ_p is the particle density, d_p is the particle diameter, and η is the average gas viscosity. The Lagrangian macro-time scale is given by,

$$T = \varepsilon / v'^2$$

where ε is the momentum eddy diffusivity and v' is the turbulence intensity. These quantities can be written in more convenient forms as,

$$\varepsilon = \mu / \rho_{air}$$

$$v'^2 = (2/3)\ K.E.$$

where μ is the turbulence viscosity and K.E. is the turbulence kinetic energy. If the properties of air are taken at standard conditions and values for μ and K.E. are taken from Regan, Chun, and Schock [18], $\tau / T = 0.0028$, which suggest that the particles are faithfully following the flow.

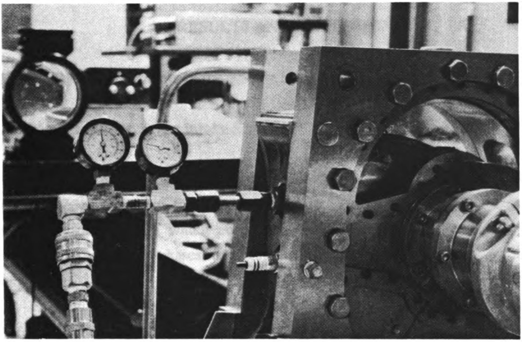

Figure 16 Pressure gauge used to measure the pressure drop across the seals

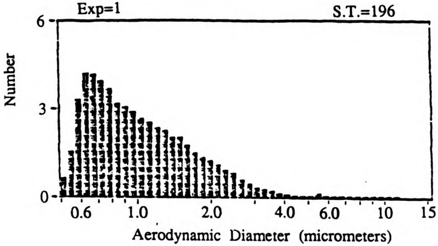

Figure 17 Particle size distribution of propylene glycol

CHAPTER 3

RESULTS AND DISCUSSION

3.1 Velocity Measurements in the Rotary Engine

3.1.1 Measurements in the Intake Stroke

Velocity measurements during the intake stroke were taken at seven locations, labeled 1-7, as shown in Figure 18. The intake flow patterns manifested themselves in three distinct phases which could be labeled early intake, mid-intake and late intake. Each of these phases has distinct characteristics which will be discussed below.

Early intake, which occurs approximately between -15 and 130 cad (see Figure 19 for reference angles), is characterized by a rotor inducted entrained fluid flow that moves toward the rotor pocket. Due to the rotor blocking the control volume, there are only three locations that indicate the flow patterns in early intake and these are locations 1, 6 and 7. Velocity plots for these locations are shown in Figures 20(a), 20(f) and 20(g), respectively. These plots indicate that the flow in early intake is predominantly along the minor axis, which is consistent with the induction action of the rotor motion. The velocity profile near the mouth of the intake port, as shown by locations 6 and 7, indicates that the inducted flow is fairly uniform across the mouth and the bulk fluid velocity is approximately 5 to 6 m/s. This trend is also shown in Figure 21(d), which combines the velocity measurements with the flow visualization results.

The mid-intake flow pattern is dominated by a large vortical structure moving counterclockwise against the rotor motion. This is caused by the interaction of the inducted flow with the blowby jet stream that moves along the housing in the opposite direction to the rotor motion. This jet is caused by the leakage past the apex seals as the compression stroke is progressing. This pattern dominates the intake flow from approximately 130 to 200 cad. The velocities at locations 1, 2 and 3 are shown in Figures 20(a), 20(b) and 20(c), and they indicate a tendency for the flow in that region to remain predominantly moving along the minor axis toward the rotor face. The velocities are higher at these locations compared to early intake velocities

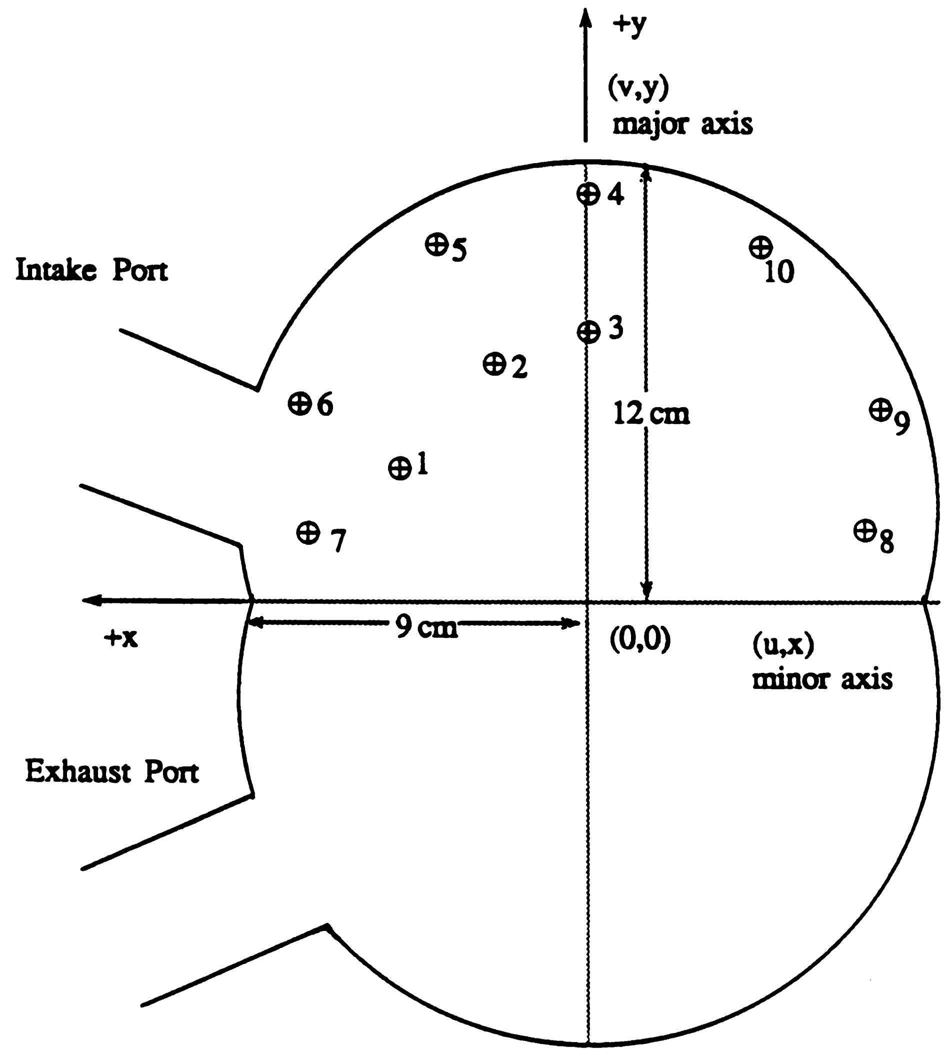

Location #	Position (mm)
1	(48.0,65.0,0.0)
2	(26.0,83.5,0.0)
3	(0.0,89.0,0.0)
4	(0.0,113.0,0.0)
5	(36.0,104.0,0.0)
6	(67.0,79.0,0.0)
7	(72.0,53.0,0.0)
8	(-72.0,53.0,0.0)
9	(-67.0,79.0,0.0)
10	(-36.0,104.0,0.0)

Figure 18 Locations for velocity measurements in the intake and compression stroke

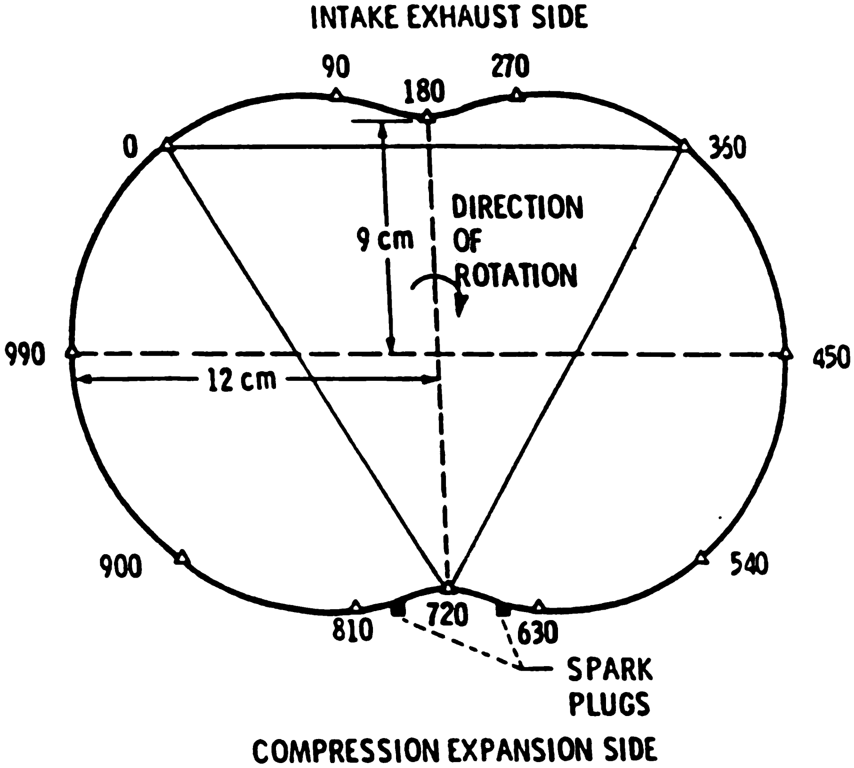

Figure 19 Reference for the crank angle degree used for the velocity plots

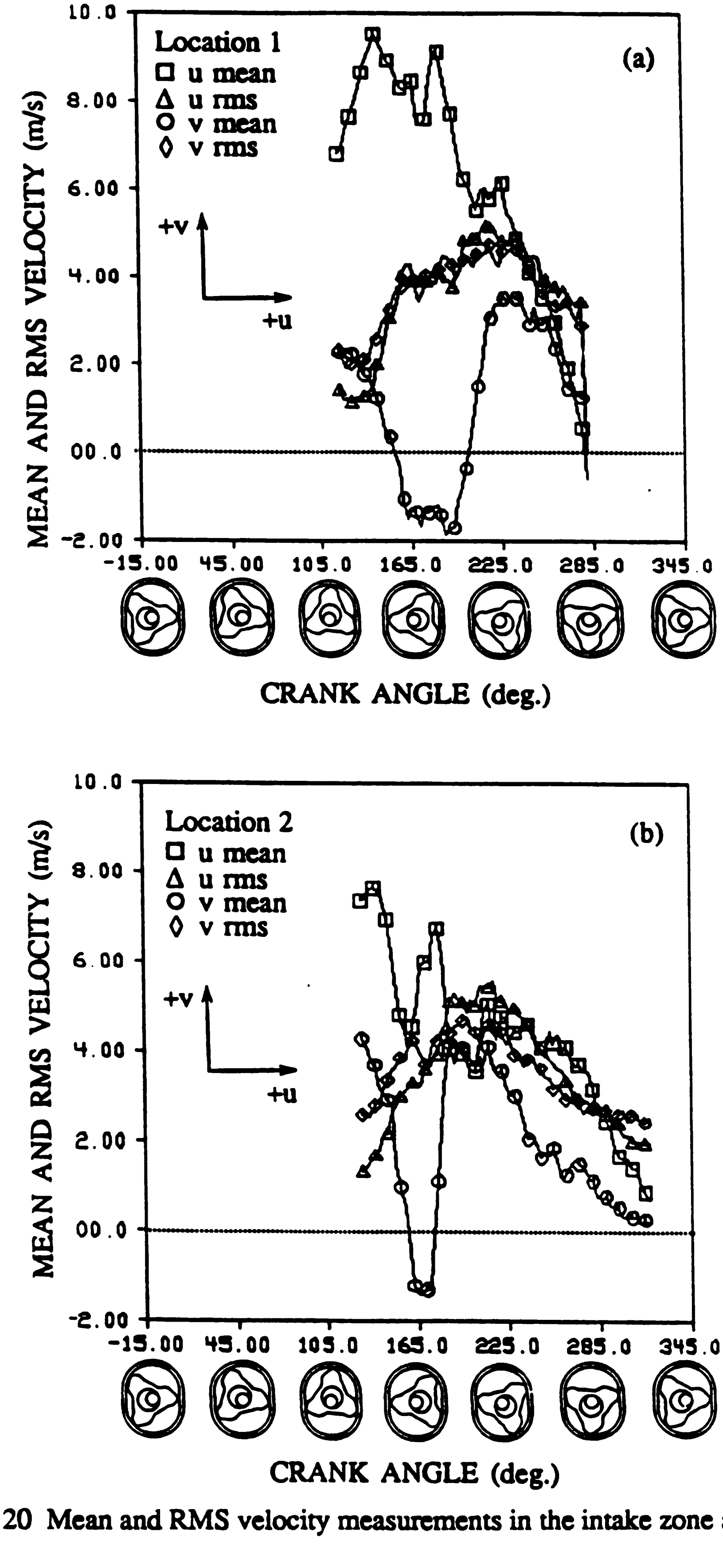

Figure 20 Mean and RMS velocity measurements in the intake zone at 675 rpm

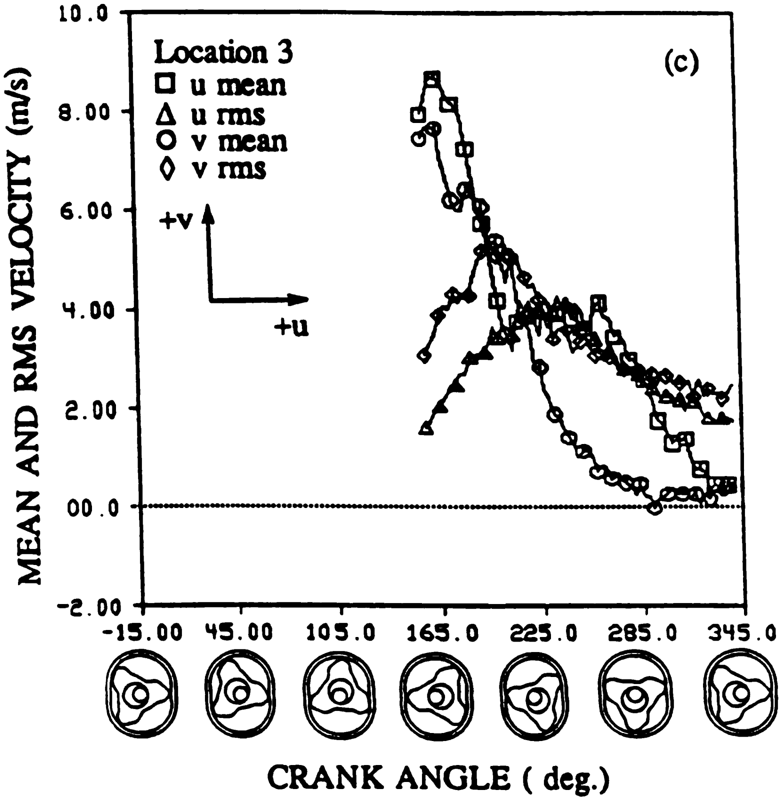

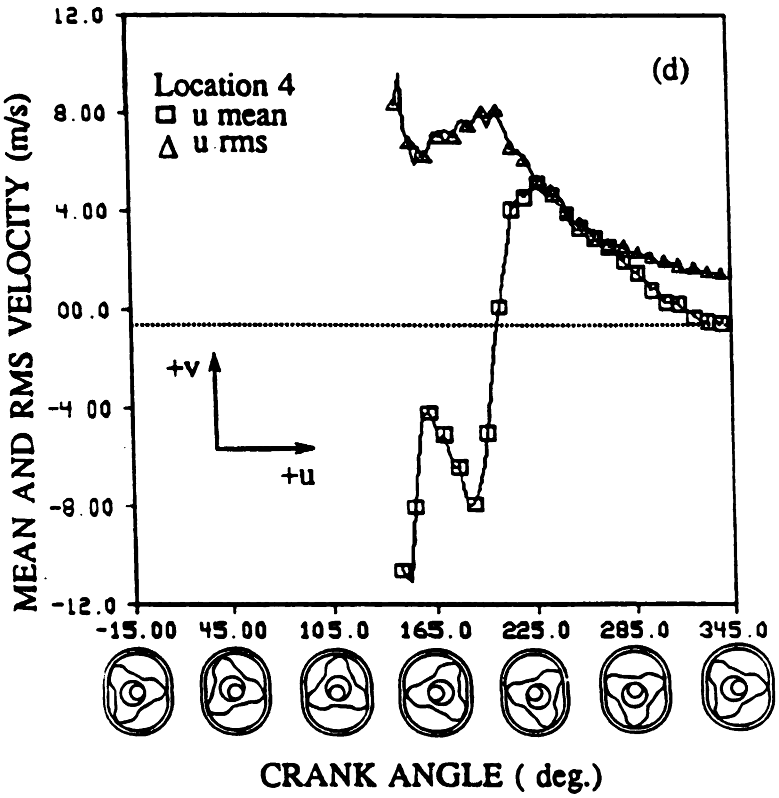

Figure 20 (cont'd)

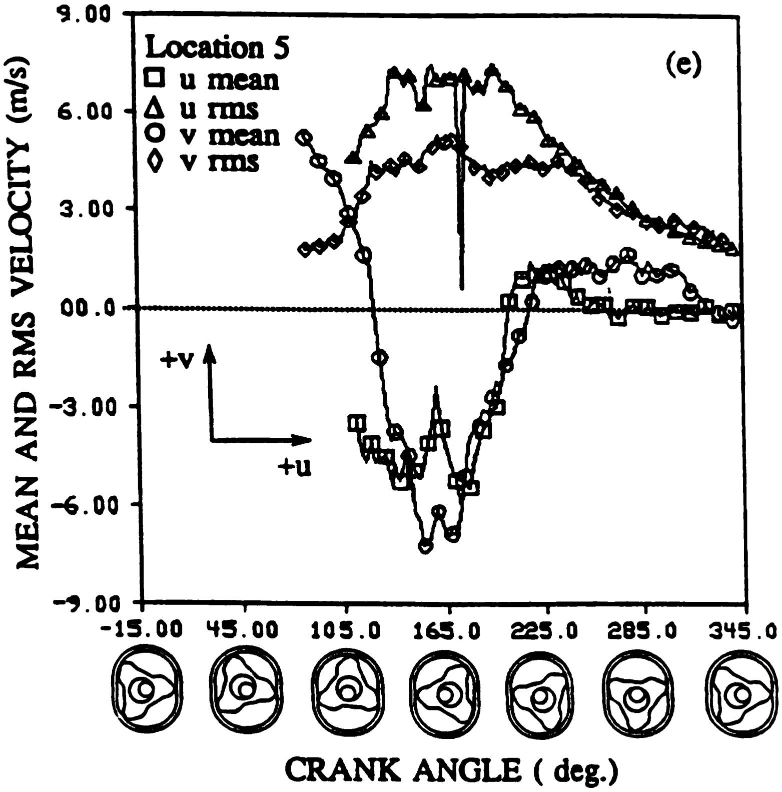

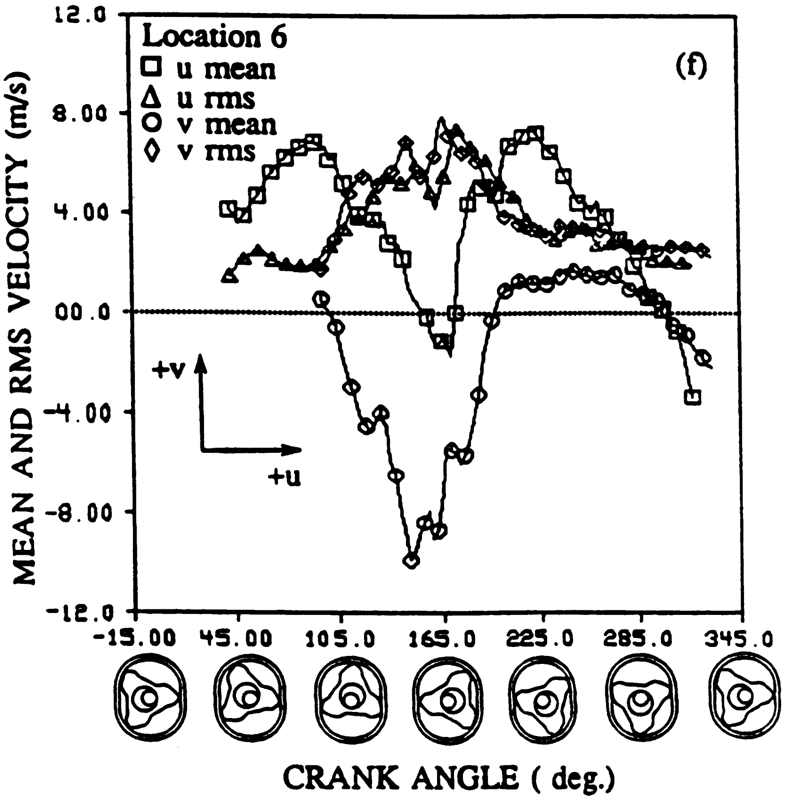

Figure 20 (cont'd)

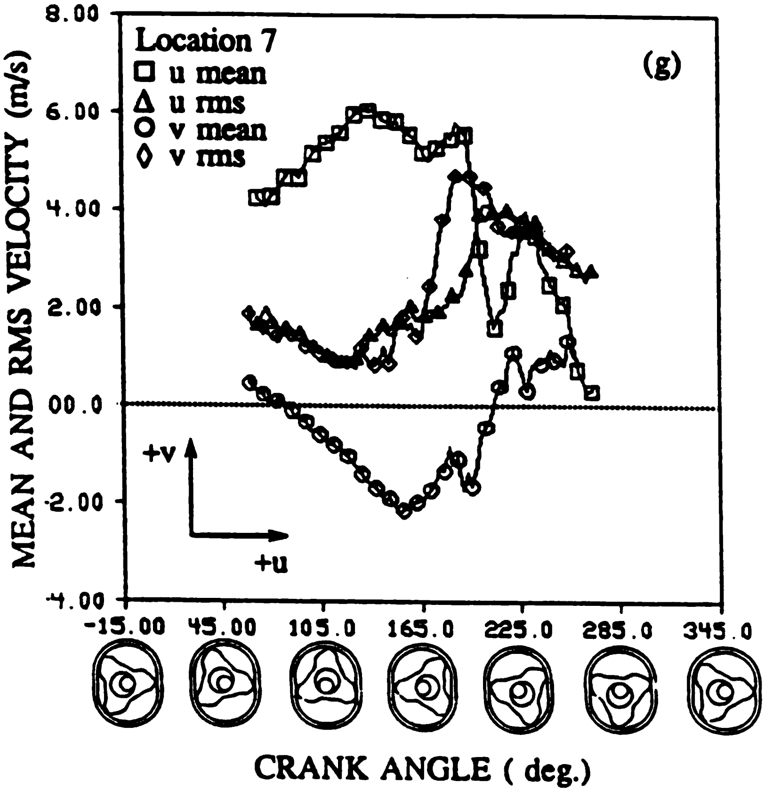

Figure 20 (cont'd)

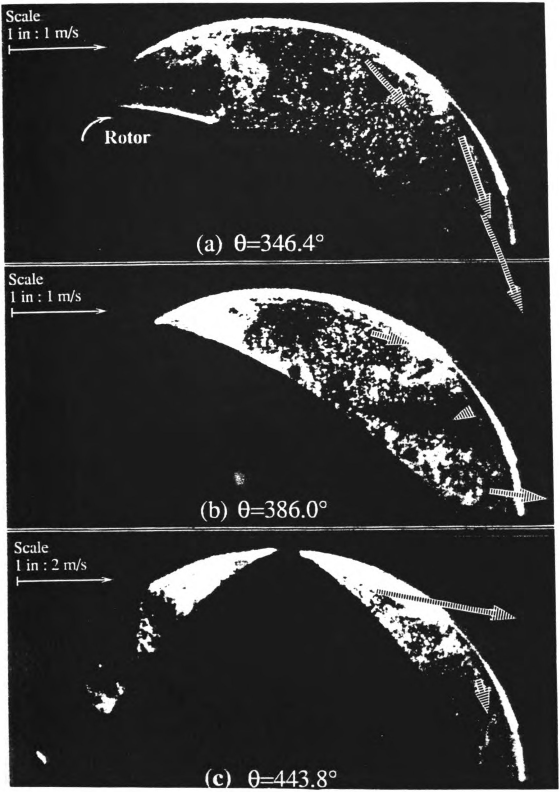

Figure 21 Velocity vectors for specified crank angles

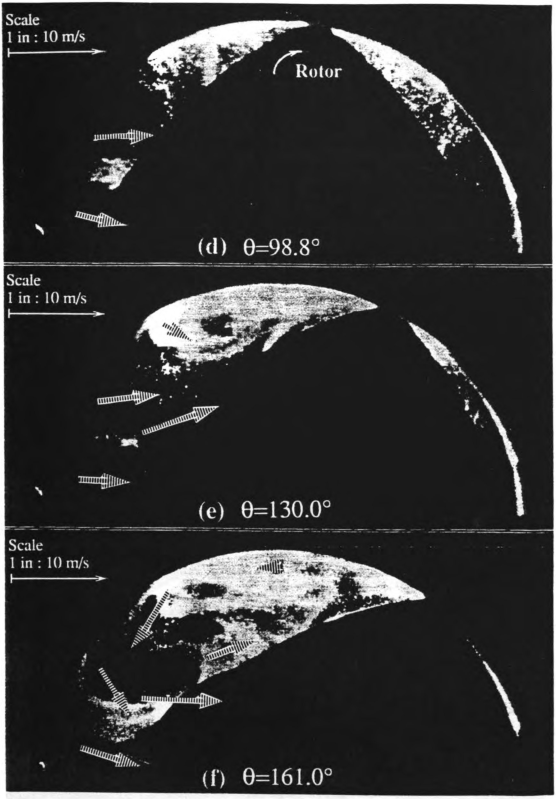

Figure 21 (cont'd)

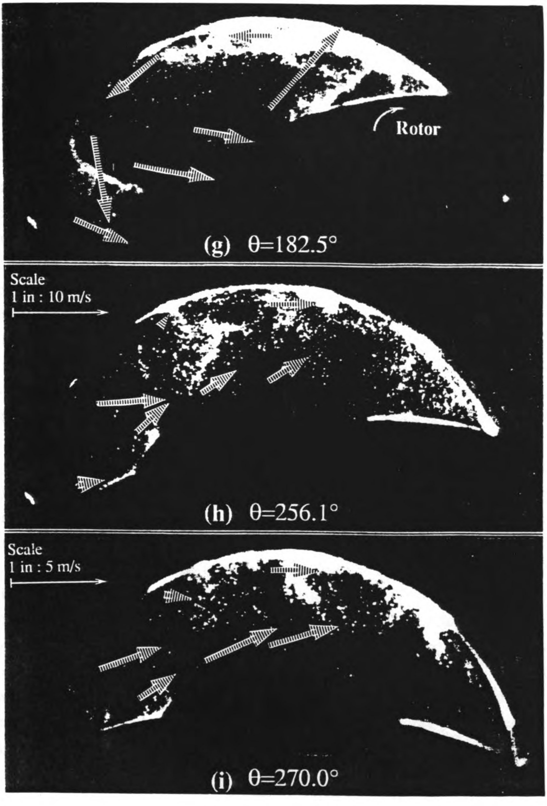

Figure 21 (cont'd)

due to the combined effects of blowby and inducted flow. The velocity measurements at locations 4, 5 and 6 are shown in Figures 20(d), 20(e) and 20(f). These plots show that as the blowby becomes more dominant the flow moving with the rotor along the central housing wall collides with the blowby jet. The inducted air flow which originally followed the rotor motion is at this time forced to reverse direction. Once the blowby flow has become fully dominant, the velocities at these locations tend to be tangent to the housing. At location 6, the blowby jet separates from the housing due to the induction flow at the intake port. These trends are remarkably shown in Figures 21(e), 21(f) and 21(g). The plot at location 5 shows a sharp decrease in the u component of the RMS velocity. This is believed to be an anomaly and not due to the physics of the actual flow.

The vortical structure caused by the blowby begins to diffuse, which takes place by turbulent mixing, into the fluid at around 200 cad. Therefore, late intake again is characterized by a rotor driven flow pattern. The velocity plots at locations 1-7 show that the u- and v-velocity components again become positive, indicating a rotor induced motion for the bulk fluid flow. The velocities also begin to decrease due to the volume rate of change reaching a minimum during late intake. Figures 21(h) and 21(i) give a good visual representation of the somewhat uniform induction flow that characterizes late intake. Figure 20(f), at location 6 near the top of the intake port, shows an interesting phenomenon that occurs when the intake and exhaust ports are overlapping. Namely, the flow reverses around 330 cad and flows around the rotor into the exhaust chamber due to a pressure gradient that is formed in the overlap region.

The RMS velocities in the intake zone generally peak in the mid-intake region due to the recirculating flow and the accompanying flow reversals. Early intake and late intake are characterized by a relative decrease in the magnitude of the RMS velocities, although the turbulence intensities in these regions are sometimes on the order of 200 to 300%. In general, the local turbulence intensities in the intake stroke were very high and irregular, which is probably a result of the highly complicated flow caused by the recirculating flow. Superposition of periodic flows such as the observed spark plug jet may also be responsible for the high turbulence intensity.

3.1.2 Measurements in the Compression Stroke

Due to difficulties with the rotor blocking the LDV signal, the velocity measurements during compression are over a relatively short range of crank angles. The flow pattern in early compression is generally moving in the direction of the rotor motion, except for flow reversals due to roll-up vortices forming on the housing boundary. Late in compression a counter-rotating flow frequently develops at the leading apex which moves toward the trailing apex in the opposite direction from the rotor motion. The "push" flow from the trailing apex then meets the counter rotating flow, which quickly reverses in the direction of the rotor. As compression progresses the flow velocities tend to increase compared to velocities in late intake and early compression, due to the fluid being driven at the speed of the rotor.

Locations 8, 9 and 10, as shown in Figure 19, indicate the positions where velocity measurements were taken in the compression zone. Figures 22(a), 22(b) and 22(c) indicate the velocity measurements at locations 8, 9 and 10 respectively. As can be seen, the v-component of velocity is generally negative due to the rotor "pushing" the fluid downward after it passes the major axis. The x-component of velocity is generally positive due to the rotor "pushing" the fluid ahead of it. Figures 21(a), 21(b) and 21(c) give a good indication of the compression flow characteristics, which are predominantly rotor driven. The flow reversal near the leading apex was not quantified due to the difficulties of taking measurements in late compression, when the reversal flow is initiated.

The RMS velocities in the compression stroke are much more uniform than what was experienced in the intake stroke. The RMS velocity seems to hover around 1.5 m/s for all three locations in the compression zone. The turbulence intensity at some crank angles is again as high as 300 to 400%, which is due to large fluctuations around a small average value.

3.1.3 Blowby Velocity Measurements

The results presented for the intake stroke indicate that blowby past the apex seal is a dominating feature in the flow pattern. Therefore, an effort was made to quantify the leakage by making measurements at the locations shown in Figure 23. In general, the results show that the blowby velocities decrease as a function of the

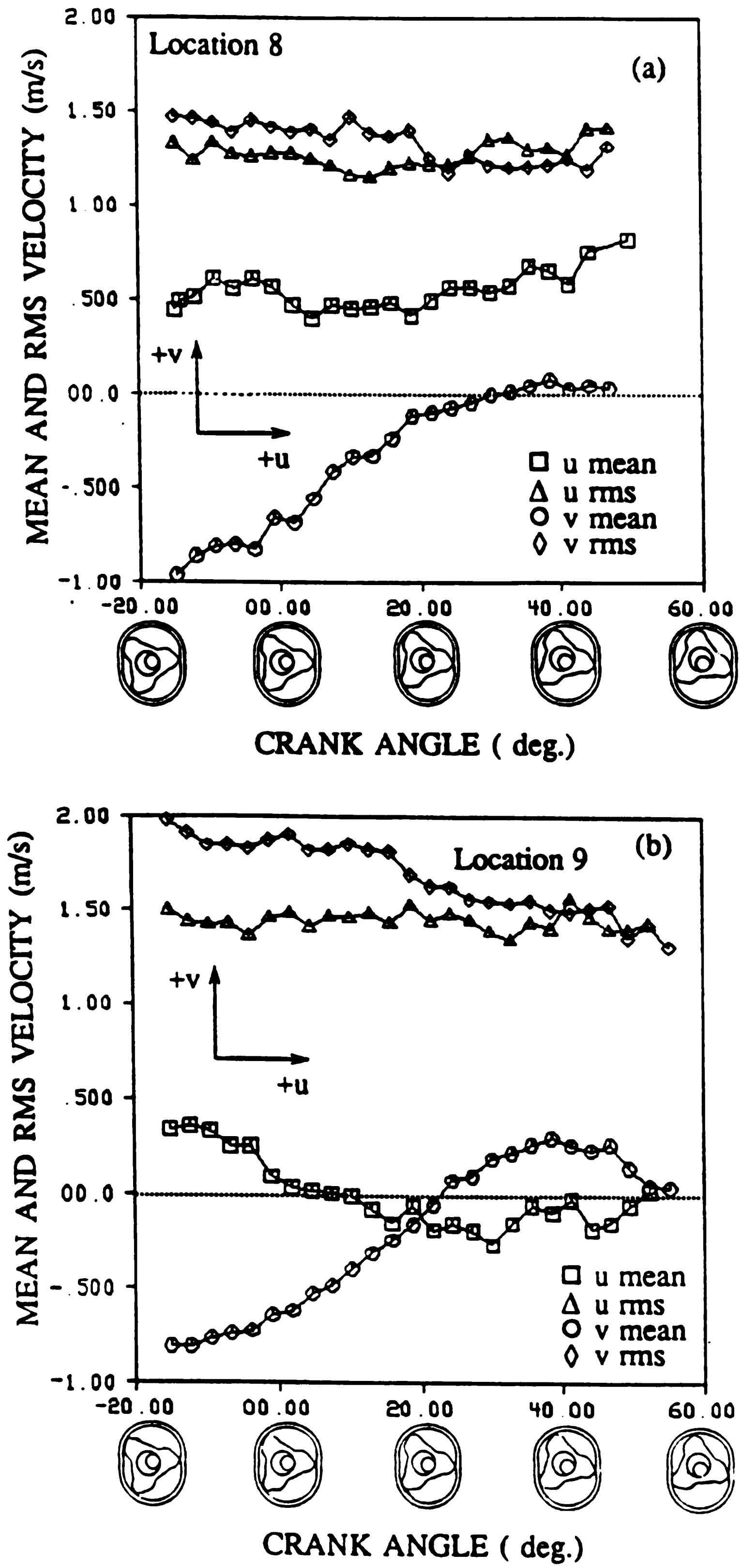

Figure 22 Mean and RMS velocity measurements in the compression zone at 675 rpm

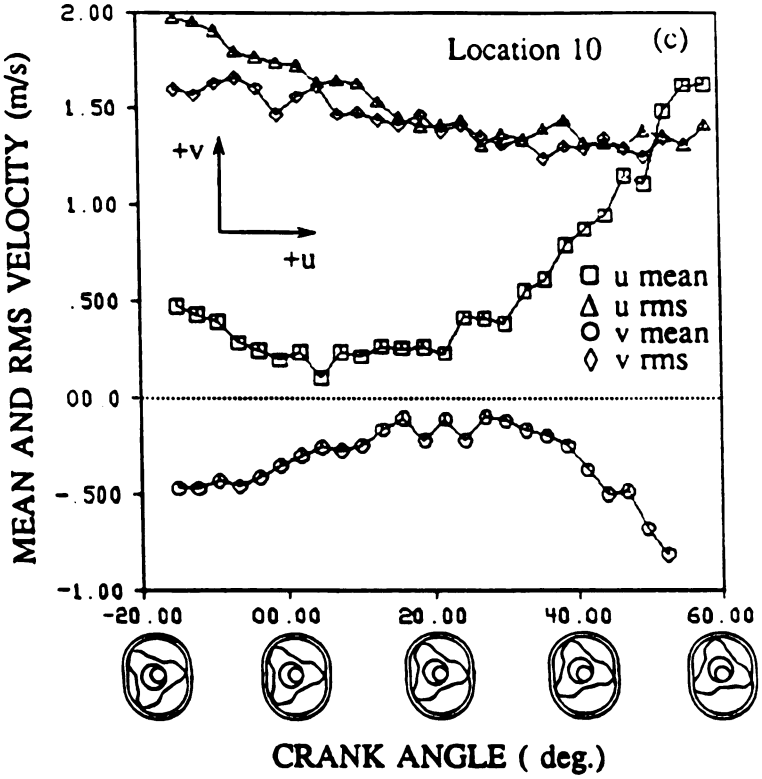

Figure 22 (cont'd)

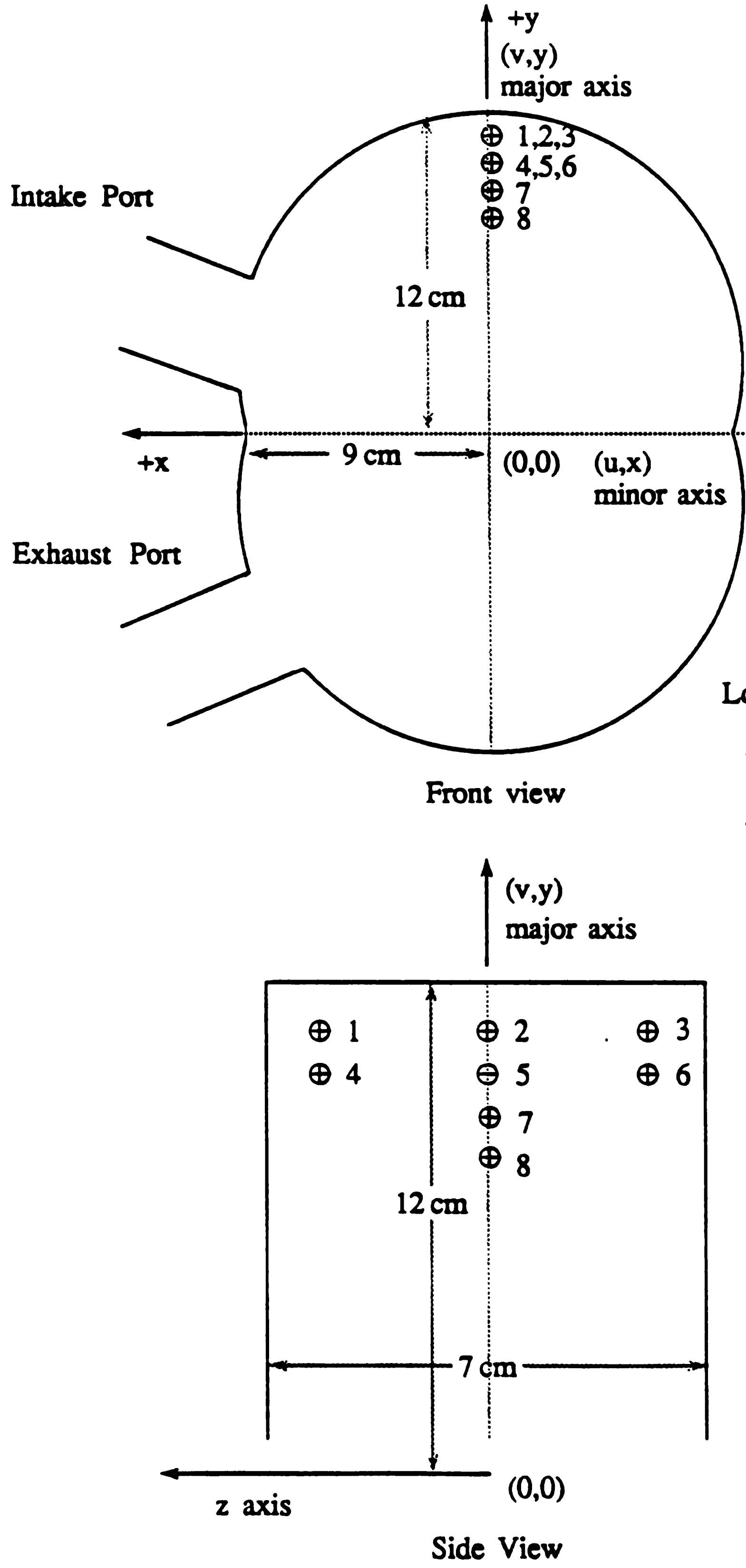

Location #	Position (mm)
1	(0.0,118.5,17.5)
2	(0.0,118.5,0.0)
3	(0.0,118.5,-17.5)
4	(0.0115.5,17.5)
5	(0.0,115.5,0.0)
6	(0.0,115.5,-17.5)
7	(0.0,113.5,0.0)
8	(0.0,111.5,0.0)

Figure 23 Location for measurements to quantify blowby

distance from the housing. Also, the plots indicate that the sealing action across the apex seal is somewhat nonuniform.

The velocity measurements taken on the center line of the housing width at varying distances from the central housing of 1.5, 4.5, 6.5 and 8.5 mm are shown in Figures 24(a), 24(b), and 24(c), respectively. These plots indicate the blowby velocity is maximum near the housing and diminishes as the distance from the housing increases, until at about 8.5 mm from the housing where the effect is minimal. The peak velocity at 1.5 mm from the housing is approximately 24 m/s which indicates that a substantial jet-type flow is being forced past the apex seals due to the pressure gradient formed across the apex seals in compression. Figures 24(a) and 24(b) show a traverse across the width of the housing at two different distances of 1.5 and 4.5 mm from the central housing wall, respectively. These plots support the contention that the seals are not sealing evenly across their length. Not only are the peak velocities different but the crank angle at which they occur are also varying in a systematic way. This suggests that one end of the apex seal is lifting off the housing at a later time. A common feature characterizing these plots is the existence of a local minimum at approximately 150 cad. This may be due to the recirculating flow impacting the blowby in the opposite direction causing a momentary velocity decrease or increase, depending on the direction of the flow near the top of the central housing when the recirculating flow arrives.

The RMS velocities are also shown and generally follow the same pattern. The RMS tends to peak at the peak mean velocity which is consistent with the jetting action of the blowby flow. The turbulence intensity tends to be on the order of 30 to 50%, although in extreme cases it was much higher.

As stated earlier, Dimpelfeld and Witze's experiment is the only other reported study which used LDV techniques to measure velocities in the rotary engine. They chose not to include frequency shifting in their system for reasons previously discussed; therefore, flow reversal measurements were not possible for their system. Figure 25 shows results presented by Dimpelfeld and Witze at a location in the intake zone, which is the approximate position of location 6 as labeled in this study and shown in Figure 18. In their study, Dimpelfeld and Witze stated that the minimum velocity at 95 cad (shown as 635 cad in their study) was somewhat difficult to explain in that this velocity occurred during the maximum rate of change of the intake zone volume. The subsequent peak in the velocity in their data is also

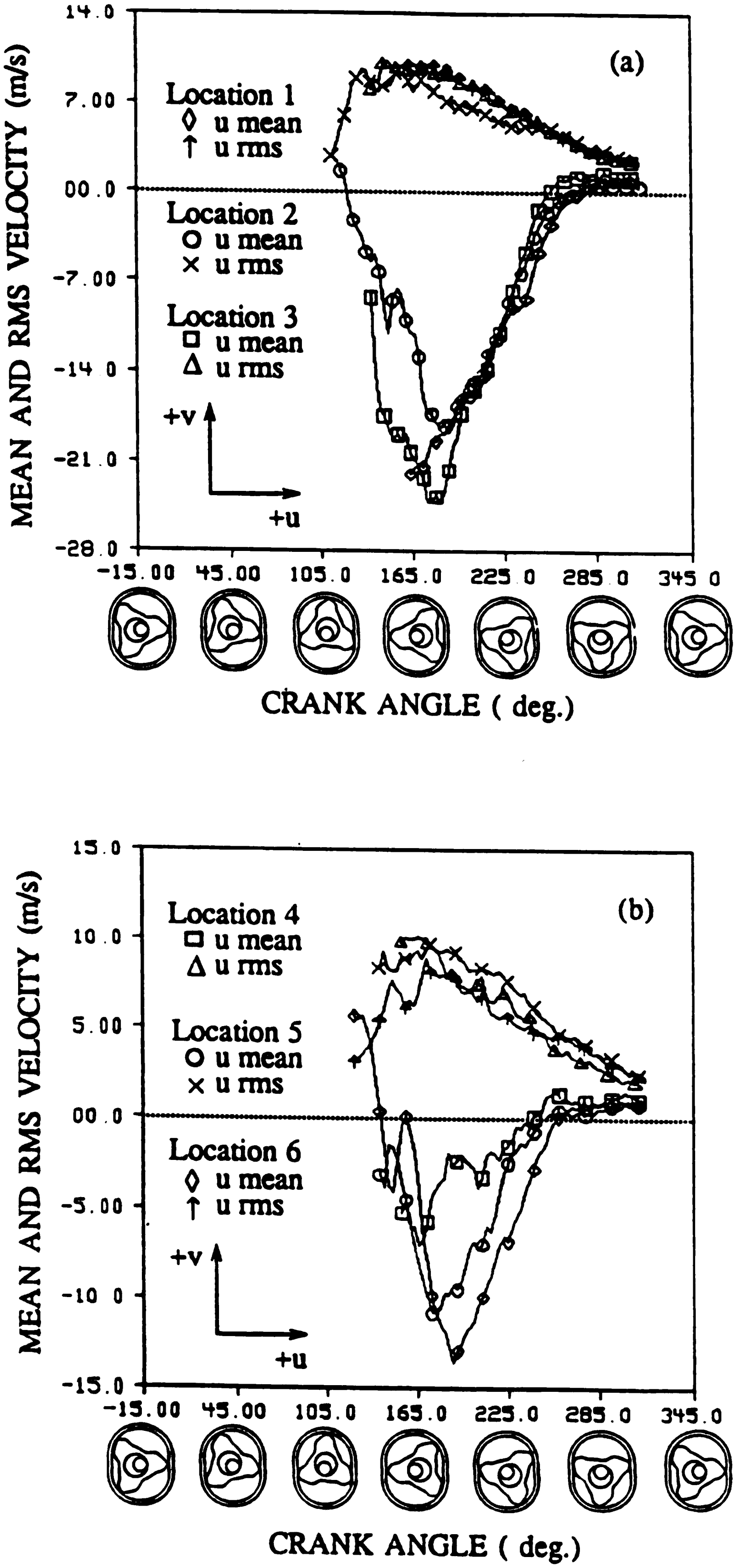

Figure 24 Mean and RMS velocity measurements to quantify blowby

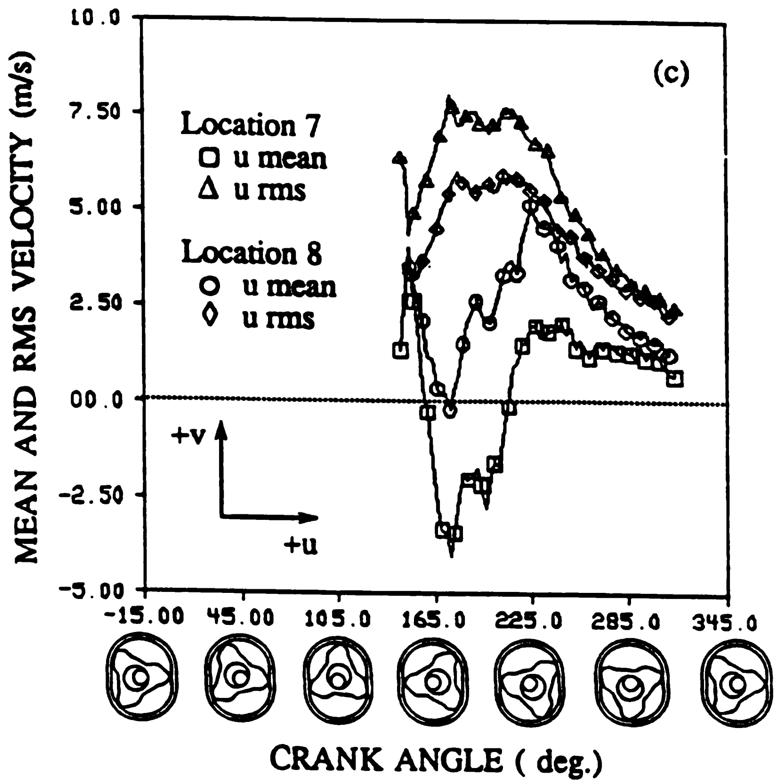

Figure 24 (cont'd)

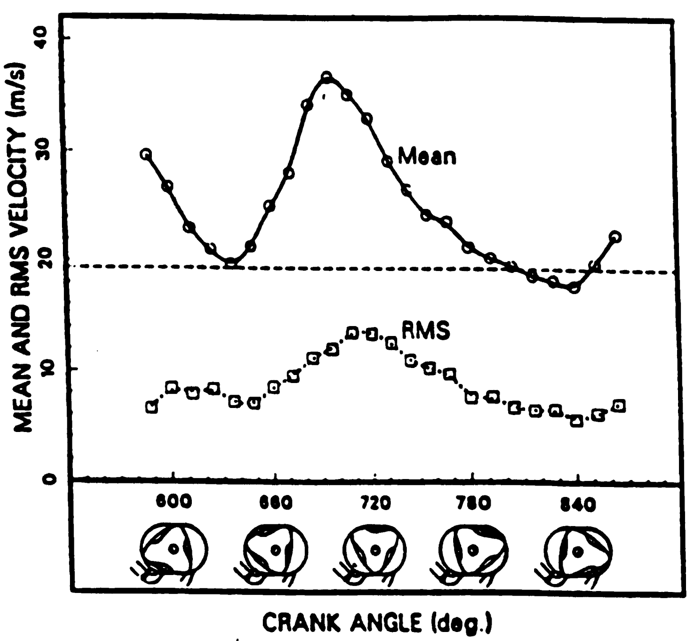

Figure 25 Velocity measurements reported by Dimpelfeld and Witze

somewhat difficult to explain from a physical standpoint; thus, the present author offers the following hypothesis. The sharp increase in velocity and its subsequent peak at 160 cad (700 cad) matches the peak in the negative flow velocity at location 6, as shown in Figure 20(f). In other words, a flow reversal as measured in the present study would appear as a positive peak in velocity in the unshifted system used by Dimpelfeld and Witze. Also, the RMS velocity plots for both studies show agreement in their general shape. It should be noted that the rotary engine used in Dimpelfeld and Witze's experiment was of a larger displacement and operated at different conditions.

3.2 Flow Visualization Results

The LDV measurements taken at 675 rpm revealed an intake flow dominated by the recirculation due to the interaction between the blowby past the apex seals and the inducted flow. This raises the issue of whether or not at higher practical operating speeds flow patterns are similar to those found at the lower speeds. Also, if the blowby is present, does it dominate the flow field as it did at the lower speed? In an attempt to address this issue, a high speed film was taken at 2000 rpm under supercharged conditions. For a description of the experimental setup and procedure see Hamady, Stuecken, and Schock [14].

The flow visualization results for 675 and 2000 rpm are shown in Figures 26 and 27, respectively. These figures reveal that the flow structures during intake and compression are preserved at the higher speeds.

The important flow structures at both operating speeds are qualitatively the same as the figures reveal. Figures 26(c) and 27(c) show that in early intake, for both 675 and 2000 rpm, the flow is directed from the intake port toward the rotor pocket. Results from both speeds show the separation near the leading apex. Figures 26(d-f) and 27(d-f) indicate that for both speeds the blowby jet is present and is progressing at the same relative rate. The figures also show that the counter clockwise recirculation flow is present for both operating conditions. Figures 26(g-i) and 27(g-i) show the flow patterns for late intake for 675 and 2000 rpm, respectively. Again, the results reveal the same general behavior for the flow field, with a diminishing of the blowby jet due to the exhaust opening and a rotor induced flow beginning to emerge.

The flow visualization results for compression again reveal that the flow

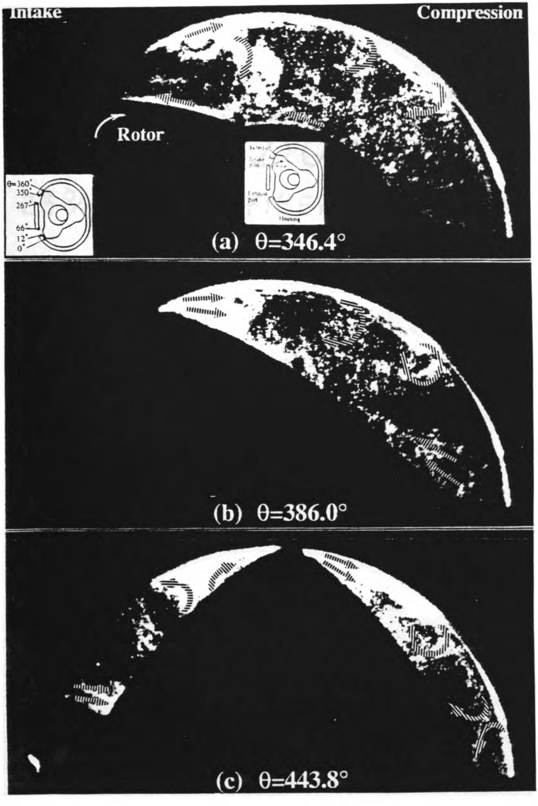

Figure 26 Flow pattern during intake and compression at 675 rpm

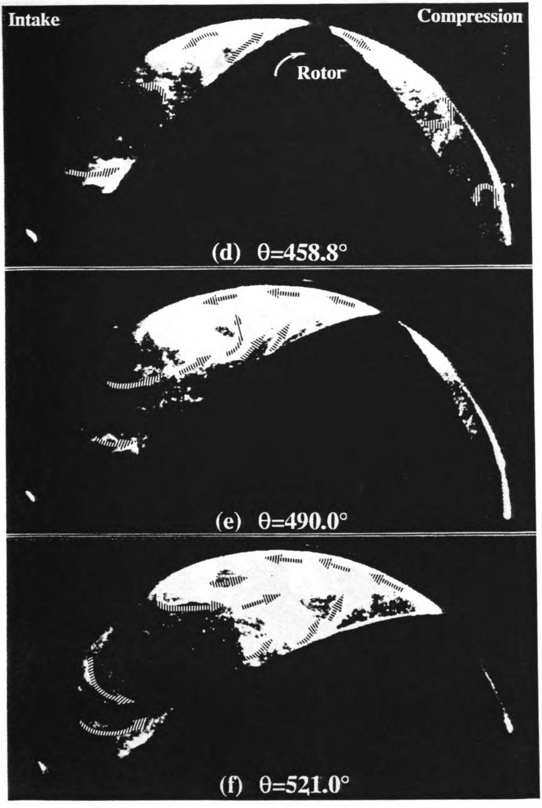

Figure 26 (cont'd)

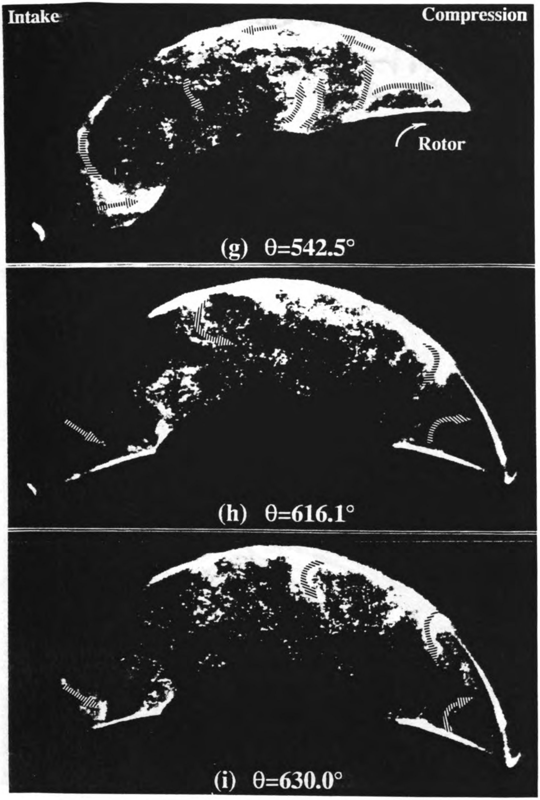

Figure 26 (cont'd)

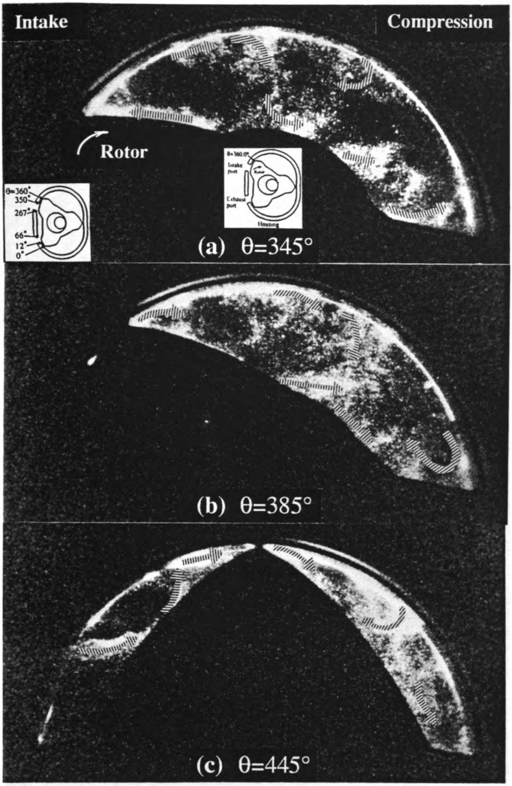

Figure 27 Flow pattern in intake and compression at 2000 rpm

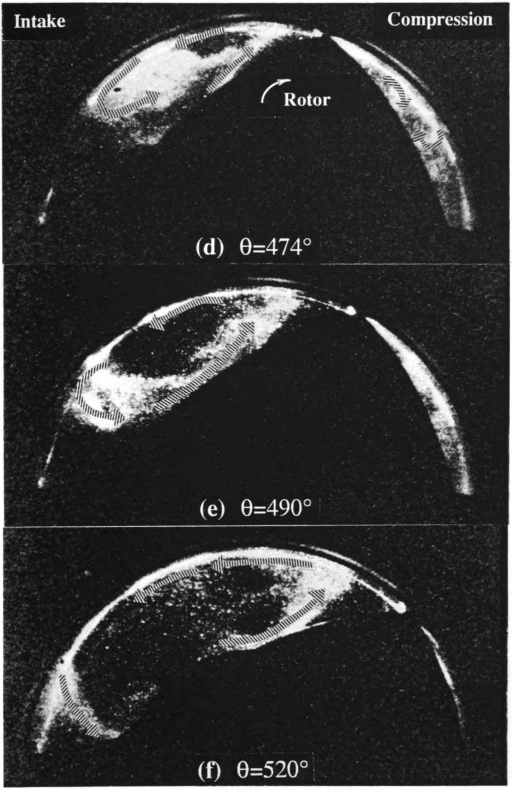

Figure 27 (cont'd)

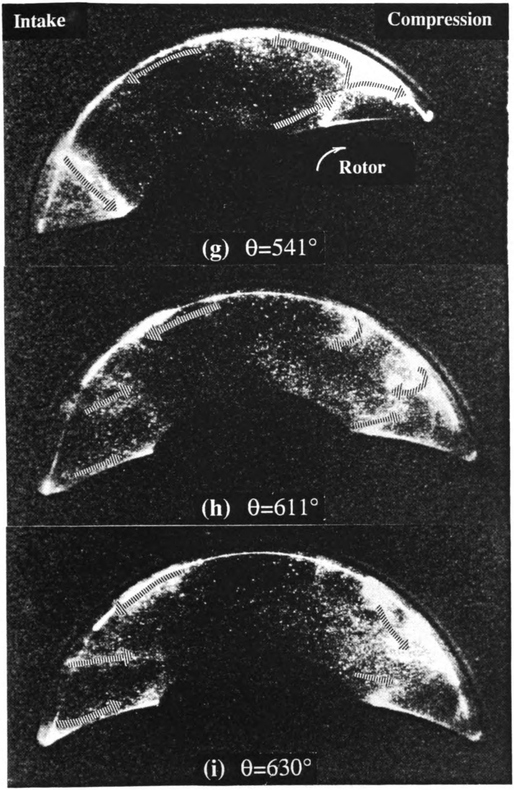

Figure 27 (cont'd)

features at the higher speeds are qualitatively the same. Figures 26(a) and 27(a) show the flow patterns in early compression for 675 and 2000 rpm, respectively. Both figures indicate the back flow along the trailing apex toward the intake port. Also, the results for both speeds show the early formation of roll-up vortices at the wall of the central housing. Figures 26(b-d) and 27 (b-d) reveal that at both speeds the flow is "pushed" ahead of the trailing apex. Also, the results show the further formation and concentration of the roll-up vortices, which are characteristic of flow behind a moving boundary (i.e. the rotor).

CHAPTER 4

SUMMARY AND CONCLUSIONS

In this investigation, LDV was used in conjunction with high speed flow visualization to quantify flow features in a motored rotary engine assembly operated at 675 rpm. In the first part of the investigation flow visualization results were used to locate flow features of interest that could be quantified using LDV measurements. Also, the flow visualization was used to verify the velocity results qualitatively. Next, flow visualization was performed at 2000 rpm to determine if the flow behavior changed significantly compared to the lower speeds. These results indicated there was no significant change in the flow field at the higher speed.

The results of the present study can be summarized as follows:

1. A dominant feature of the flow during the intake stroke is the recirculation due to the blowby past the apex seals. The blowby causes the intake flow to be highly irregular and the turbulence intensities to be very high.

2. The flow during the compression stroke was shown to be predominantly rotor "pushed", although flow reversals were seen in the form of roll-up vortices and back flows.

3. The LDV velocity measurements in the rotary engine confirmed the existence of blowby past the apex seals that was seen in the high speed films.

4. The high speed film taken at 2000 rpm indicated that the flow field at the higher speed was qualitatively the same as the flow field seen at 675 rpm.

CHAPTER 5

RECOMMENDATIONS

In order to continue the progress toward a better designed rotary engine, these recommendations for future work seem appropriate.

1. The results of this study indicate the importance of further work on apex sealing systems. New seal designs and experiments at high speed conditions must be coupled with numerical models to improve the engine design. However, regardless of the direction that the design process takes, the seal leakage will most likely be an important consideration.

2. The flow patterns in compression must be thoroughly mapped in order to determine how the flow is behaving and how this behavior affects the fuel injection and combustion process.

3. If rotary engines with advanced sealing systems have leakage as this study suggests, numerical simulation will have to be modified to include the effect of blowby. This will necessitate the simultaneous modeling of three combustion chambers rather than the single combustion chamber currently being used.

In an attempt to accomplish some of these goals, LDV measurements were attempted at the higher speeds. However, over heating in the shaft bearings made this impossible. Currently, work is being done to modify the bearings to allow lubrication during operation. Also, the side housings are being coated with a ceramic material to allow the engine to run with production metal seals. This should allow for higher speed operation and enable LDV measurements to be taken at the higher speeds with a conventional sealing system.

REFERENCES

LIST OF REFERENCES

1. Hamady, F.J., Kosterman, J., Chouinard, E., Somerton, C., Schock, H.J., Chun, K. and Hicks, Y., "Stratified Charge Rotary Engine Internal Flow Studies at the MSU Engine Research Laboratory," SAE Paper No. 890331, 1989.

2. Bayer, R.J., DeNagel, S.F., and Steiner, J.C., "Rotary Combustion Engine Hydrocarbon Source Studies," SAE Paper No. 780965, SAE Transactions, Vol. 87, Section 4, pp. 3619-3636, 1979.

3. Kohno, J., Ito, R., Monta, M. and Mizuno, N., "Analysis of Light-Load Performance in Rotary Engines," SAE Paper No. 790435, SAE Transactions, Vol. 88, Section 2, pp. 1637-1652, 1980.

4. Lamping, R.K., Manning, I., Myers, D. and Tjoa, B., "Performance, Emissions and Physical Characteristics of Rotating Combustion Aircraft Engine," NASA CR-1351119, Supplement A, May 1980.

5. Eberle, M.K. and Klomp, E.D., "An Evaluation of the Potential Performance Gain from Leakage Reduction in Rotary Engines," SAE Paper No. 730117, SAE Transactions, Vol. 82, pp. 454-460, 1974.

6. Knoll, J., Vilmann, C. R., Schock, H. J. and Stumpf, R. P., "A Dynamic Analysis of Rotary Combustion Engine Seals," SAE Paper No. 840035, 1984.

7. Meng, P.R., Rice, W.J., Schock, H.J. and Pringle, D.P., "Preliminary Results on Performance Testing of a Turbocharged Rotary Combustion Engine," SAE Paper No. 820354, 1982.

8.. Bracco, F.V. and Sirignano, W.A., "Theoretical Analysis of Wankel Engine Combustion," Combust. Sci. Technol., Vol. 7, pp. 69-84, 1973.

9. Shih, T. I-P., Yang, S.L., and Schock, H. J., "A Two-Dimensional Numerical Study of the Flow Inside the Combustion Chamber of a Motored Rotary Engine," SAE Paper No. 860615, 1986.

10. Shih, T. I-P., Schock, H.J. and Ramos, J.I., "Fuel-Air Mixing and Combustion in a Two-Dimensional Wankel Engine," SAE Paper No. 870408, 1987.

11. Steinthorsson, E., Shih, T. I-P., Schock, H.J. and Stegeman, J., "Calculation of the Unsteady, Three Dimensional Flow Field Inside a Motored Wankel Engine," SAE Paper No. 880625, 1988.

12. Hicks, Y.R., Schock, H.J., Craig, J.E, Umstatter, H.L. and Lee, D.Y., "Visualization of Flows in a Motored Rotary Combustion Engine Using Holographic Interferometry,' AIAA Paper 86-1557, 1986.

13. Dimpelfeld, P.M. and Witze, P.O., "Velocity Measurements in a 5.8 Liter Stratified-Charge Rotary Engine," Sandia National Laboratories, July 1988.

14. Hamady, F.J., Stuecken, T., and Schock, H.J., "Airflow Visualization and LDV Measurements in a Motored Rotary Engine Assembly Part 1: Flow Visualization", SAE Paper No. 900030, 1990.

15. TSI, INC., "Rotating Machinery Software Program", Users Manual, 1988.

16. Mazda Motor Co., "Mazda RX-7 Workshop Manual", Repair Manual, 1984.

17. TSI, INC., "Model 9306 6-Jet Atomizer", Instruction Manual, 1987.

18. Regan, C.A., Chun, K.S. and Schock, H.J., "Engine Flow Visualization Using Copper Vapor Laser," Proceedings of SPIE, Vol. 737, pp. 17-27, 1987.